

2018-10-01

Analytical study on wave power extraction from a hybrid wave energy converter

Zheng, Siming

<http://hdl.handle.net/10026.1/12010>

10.1016/j.oceaneng.2018.07.021

Ocean Engineering

Elsevier

All content in PEARL is protected by copyright law. Author manuscripts are made available in accordance with publisher policies. Please cite only the published version using the details provided on the item record or document. In the absence of an open licence (e.g. Creative Commons), permissions for further reuse of content should be sought from the publisher or author.

1 **Title:**

2 Analytical study on wave power extraction from a hybrid wave
3 energy converter

4

5 **Author names and affiliations:**

6 Siming Zheng

7 *State Key Laboratory of Hydrosience and Engineering, Tsinghua University, Beijing 100084,*
8 *China*

9 *E-mail address: zhengsm@tsinghua.edu.cn*

10

11 Yongliang Zhang

12 *State Key Laboratory of Hydrosience and Engineering, Tsinghua University, Beijing 100084,*
13 *China*

14 *E-mail address: yongliangzhang@tsinghua.edu.cn*

15

16 **Corresponding author:**

17 Yongliang Zhang

18 *State Key Laboratory of Hydrosience and Engineering, Tsinghua University, Beijing 100084,*
19 *China*

20 *Tel.: + 86 10 62797802*

21 *E-mail address: yongliangzhang@tsinghua.edu.cn*

22

23 Accepted 8 July 2018

24 <https://doi.org/10.1016/j.oceaneng.2018.07.021>

1 Analytical study on wave power extraction from a hybrid wave 2 energy converter

3 Abstract: In this paper, a hybrid wave energy converter (WEC) is proposed, consisting of a fixed
4 inverted flume with long length and a bottom hole, and a long floating cube hinged with the
5 flume. The inverted flume and the long floating cube works as an oscillating water column
6 (OWC) and a rotational float, respectively, to capture power from incident waves. To study the
7 performance of this hybrid WEC, analytical solution of the wave diffraction/radiation problems,
8 considering the hydrodynamic interaction between the OWC and the float, is derived based on
9 linear potential flow theory and eigen-function expansion matching method in the two-
10 dimensional Cartesian coordinate systems. The corresponding hydrodynamic coefficients, such as
11 wave excitation forces, added mass and wave radiation damping, are also obtained, which can be
12 further used in evaluation of the maximum theoretical power absorption of the hybrid WEC.
13 Results are compared with a parallel study of an isolated OWC and an isolated float.
14 Additionally, analytical study on power capture capability of the device for various geometrical
15 parameters is then carried out.

16 Keywords: Linear potential flow theory, Analytical model, Wave power extraction, Oscillating
17 Water Column, Hinged float

18 1. Introduction

19 Oscillating water column (OWC) has been recognized as one of the most effective concepts of
20 wave energy conversion, which mainly consists of a partially submerged rigid chamber and
21 exploits wave power by driving an air turbine using the oscillating motion of the inner free water
22 surface (Heath, 2012; Malara and Arena, 2013; Deng et al., 2014; He and Huang, 2017; Chen et
23 al., 2017). To understand and improve wave power extraction by OWC devices, experimental,
24 numerical, and analytical methods have been widely employed and many different design of
25 OWC devices have been proposed as well.
26 Experimental tests present a straightforward way to study the performance of OWC devices. For
27 the case where the OWC is very long in the horizontal co-ordinate compared to the wave length,
28 wave diffraction and radiation from the OWC can be concerned with a two-dimensional problem.
29 Sarmiento (1992) carried out wave flume experiments on two-dimensional OWC devices and
30 found a good agreement between the experimental data and the prediction values from linear
31 theory. Morris-Thomas et al. (2007) experimentally studied a shore based oscillating OWC
32 device, and found that the increase in front wall submergence reduced the power capture
33 efficiency in short waves. He et al. (2013, 2017) considered the integration of OWC devices with
34 a floating breakwater, which was experimentally found to be a promising way to widen the
35 frequency range for power extraction. Due to the constraints of laboratory facilities, funding and
36 time in conducting experimental studies of OWC devices, numerical and analytical methods were
37 preferred by many researchers.
38 Numerical studies on OWC devices are commonly performed by using BEM (Boundary Element
39 Method) models and RANS (Reynolds-Averaged Navier-Stokes equations) models, which are
40 based on potential flow theory and viscous fluid theory, respectively. Sheng et al. (2014) used an
41 imaginary “piston” to replace part of the water at the internal water surface in the OWC chamber
42 and solved the hydrodynamic problems from the device itself and the imaginary “piston” by using
43 a commercial BEM model. Appropriate representation of the “imaginary” piston was found very

1 important, when the hydrodynamic parameters were to be transformed from frequency-domain to
2 time domain for a further analysis. Rezanejad et al. (2013, 2015) adopted BEM method to analyse
3 the efficiency of a two-dimensional nearshore multiple OWC devices placed over flat bottom and
4 stepped bottom, respectively. Ning et al. (2015, 2017) applied a fully nonlinear numerical wave
5 flume based on higher-order BEM in simulating of both one-chamber and dual-chamber OWC
6 devices. Numerical results indicated that the surface elevations in the two sub-chambers are
7 strongly dependent on the wave conditions. Compared with BEM models, the RANS models are
8 capable to handle problems with very strong nonlinearity induced by turbulence, viscous, vortex
9 shedding and wave breaking. Elhanafi et al. (2016, 2017) used a fully nonlinear 2D RANS model
10 to carry out analysis of onshore and offshore OWC devices, respectively. Frequency response of
11 the overall hydrodynamic efficiency showed a single-peaked curve and it was revealed that
12 increase of the submergence of lips was beneficial to the energy extraction in long waves,
13 whereas went against power absorption for short waves. Other numerical investigations on OWC
14 devices with implementation of RANS models can be found in Zhang et al. (2012), López et al.
15 (2014, 2016), Iturrioz et al. (2015). However, as the RANS model utilized in the above-
16 mentioned numerical simulations normally requires a much more computational power, its
17 employment is limited to a certain extent in some ways.

18 For the OWCs in regular shapes, the analytical method, which is generally based on potential
19 flow theory and eigen-function expansions, can be a good alternative option, especially in their
20 pre-feasibility study and even their feasibility study, and can be used to provide insights and
21 important information rapidly at relatively low costs.

22 As early as 1980s, Evans (1982) presented theoretical results of wave-power absorption by a two-
23 dimensional system of uniform oscillatory surface pressure distributions based on the linearized
24 hydrodynamic theory. Later, Falnes and McIver (1985) applied analytical method to study the
25 power absorption by an OWC, which is composed of two vertical barriers with unequal length,
26 oscillating in the surge mode. It was shown that all of the incident wave power can be captured by
27 the system with optimum values of the complex oscillation amplitudes. Sarmiento and Falcão
28 (1985) developed an analytical analysis for an OWC device in which the immersed part of the
29 OWC was assumed of shallow draught. Evans and Porter (1995) described an accurate model
30 using matched eigen-function expansions and a Galerkin method to compute the hydrodynamic
31 coefficients associated with an OWC device consisting of a thin vertical surface-piercing barrier
32 next to a vertical wall. This method has been widely used in solving the hydrodynamic problems
33 of the OWC based on thin barrier assumption. It was found that the OWC with a larger chamber
34 width had a smaller wave frequency at which resonance occurs. Rezanejad et al. (2013) studied
35 the performance of a dual-chamber OWC device which consists of two vertical thin barriers in
36 front of a vertical wall. It was revealed that the draft of the outside chamber was a dominant
37 parameter determining the basic resonance frequency of power extraction. Later, the dual-
38 chamber OWC with vertical thin barriers placed over stepped bottom was also analysed
39 (Rezanejad et al., 2015). Noad and Porter (2017) considered a simplified model of a shallow-
40 draughted multiple-chamber OWC which is comprised of a series of open bottomed chambers
41 each enclosing an internal free surface. It was identified that variations in chamber sizing were
42 advantageous, with larger chambers positioned to the aft, not only dividing the power capture
43 more evenly between the chambers, but also leading to a broader-banded response. As another
44 development of the simple OWC, the U-OWC device utilizing a small vertical U-duct for
45 connecting the air pocket to the open wave field was introduced and its performance was
46 analytically investigated by Boccotti (2007) and Malara and Arena (2013). While due to either
47 “thin barrier” or “shallow draught barrier” assumptions, the analytical models proposed so far are
48 not valid in dealing with a more common situation, where the thickness and draught of the OWC
49 chamber cannot be ignored. Although Zheng and Zhang (2016) have recently developed an
50 analytical model for diffraction and radiation problems of multiple floats, in which any two
51 adjacent floats might be seen as the fore and aft walls of OWC with arbitrary thickness, the

1 radiation problem due to pressure oscillation inside the OWC chamber has not been taken into
2 account.

3 This paper extends the previously mentioned traditional offshore OWC concept, discussed by
4 Elhanafi et al. (2017), by considering a long oscillating floating cube hinged onto the OWC. The
5 aim is to enhance the performance of overall wave energy absorption. Apart from harnessing
6 power by the air turbine at the top of the OWC, rotation of the float (the long oscillating floating
7 cube) relative to the OWC can also be adopted to drive a cylinder installed between the OWC and
8 float, extracting wave power. Therefore, the device might be named as a hybrid wave energy
9 converter (WEC). On the one hand, due to the physical connection of the oscillating float onto the
10 OWC, no mooring system is required for the float and the costs of construction could be reduced.
11 On the other hand, it is believed that, with an optimized dimension, power extraction of the
12 hybrid WEC can be obviously improved for a large range of wave frequencies due to the
13 hydrodynamic interaction between the OWC and oscillating float. To study the hydrodynamic
14 performance of the hybrid WEC, the previously mentioned analytical model for the diffraction
15 and radiation problem from multiple floats, discussed by Zheng and Zhang (2016) is extended by
16 considering the radiation due to pressure oscillation between two adjacent floats, and then
17 employed to carry out a geometric parametric study of the hybrid WEC. Results are compared
18 with a parallel study of an isolated OWC and an isolated float.

19 The rest of the paper is organized as follows. Section 2 describes the analytical model used in the
20 hydrodynamic simulations. Section 3 presents the validation of the analytical model. Results and
21 discussions are provided in Section 4. Conclusions are summarized in Section 5.

23 **2. Analytical model**

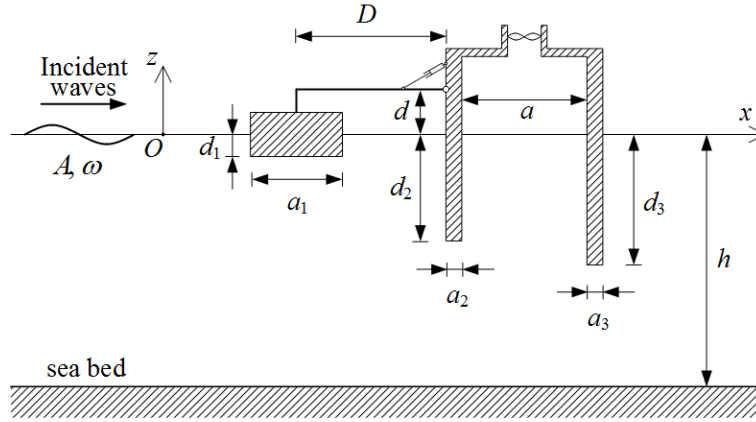
24 **2.1. Problem description**

25 The hybrid WEC proposed is mainly composed of a fixed OWC chamber and a float, as shown in
26 Fig. 1. The float is connected to the fore wall of the OWC through a rigid arm. As ocean waves
27 pass through the hybrid WEC, the OWC can be used to drive an air turbine and a motor installed
28 at the top of the OWC chamber to capture wave power. Additionally, the wave-induced rotation
29 of the float around the hinge can be employed to drive a hydraulic cylinder installed between the
30 rigid arm and the OWC to exploit wave power as well.

31 It is assumed that the monochromatic incident waves of small amplitude A and frequency ω
32 propagate perpendicularly to the WEC and the length of the hybrid WEC along the crest line of
33 these incident waves is much larger than wave length. Therefore, wave diffraction/radiation
34 problems of this WEC can be treated as two-dimensional ones. As given in Fig. 1, a Cartesian
35 coordinate (x, z) system with its original point O located at the point of intersection of the mean
36 water surface and the front wall of the float is used to formulate the hydrodynamic problem of the
37 hybrid WEC, in which x and z denote the incident wave propagation and the upward direction,
38 respectively. The width of the float, the thickness of the fore wall and aft wall of OWC chamber
39 are denoted as a_1 , a_2 and a_3 , respectively. The draft of the float, the submergence of the fore wall
40 and aft wall of OWC chamber are denoted as d_1 , d_2 and d_3 , respectively. a represents the water
41 column width inside the OWC chamber; d denotes the height of the hinge relative to the mean
42 water surface; D represents the distance between the float center and the fore wall of OWC. The
43 water area is considered with a constant depth of h . As shown in Fig.1, if we choose the hinge

1 point as a reference point of the float motion, the floater has only one degree of freedom, i.e. pitch
 2 rotation relative to the hinge point. In such situation, the excitation pitch moment and the
 3 hydrodynamic coefficients in rotation mode of the float are strongly dependent on the height of
 4 the hinge relative to the mean water surface, i.e. d . In this paper, the center of gravity of the float
 5 (x_0, z_0) is used as the reference point to calculate the motion response of the float. Hence surge,
 6 heave and pitch modes should all be considered in solving wave diffraction and radiation
 7 problems. The mechanical relation between the surge/heave and pitch modes induced by the
 8 hinge constraint can be further taken into account in evaluating motion response of the WEC
 9 without resolving hydrodynamic problem for different d .

10



11

12

Fig. 1. Definition sketch of the hybrid WEC

13 In common with the assumptions that have been adopted by Zheng and Zhang (2016), in this
 14 paper, the fluid is considered isotropic and incompressible inviscid, the time-harmonic flow is
 15 irrotational, and the deformation of both float and OWC chamber are neglected.

16 With the employment of linear potential flow theory, the fluid motion can be expressed by the
 17 velocity potential $\varphi = \text{Re}[\Phi(x, z)e^{-i\omega t}]$, where Φ is a complex spatial velocity potential
 18 satisfying the Laplace equation; i is the imaginary unit and t is the time.

19 Φ can be decomposed into an incident wave spatial potential Φ_I , a diffracted wave spatial
 20 potential Φ_D and four radiated wave spatial potential $\Phi_R^{(L)}$:

$$21 \quad \Phi = \Phi_I + \Phi_D + \sum_{L=1}^3 \dot{A}_L \Phi_R^{(L)} + p \Phi_R^{(4)}, \quad (1)$$

22 where \dot{A}_L is the complex amplitude of the float velocity oscillation in mode L ($L=1, 2, 3$, which
 23 represent surge, heave and pitch, respectively); $\Phi_R^{(L)}$ ($L=1, 2, 3$) is the spatial velocity potential
 24 due to unit amplitude velocity oscillation of the float in mode L ; p is the complex air pressure

1 amplitude inside the OWC chamber; $\Phi_R^{(4)}$ is the spatial velocity potential due to unit air pressure
 2 oscillation inside the OWC chamber.

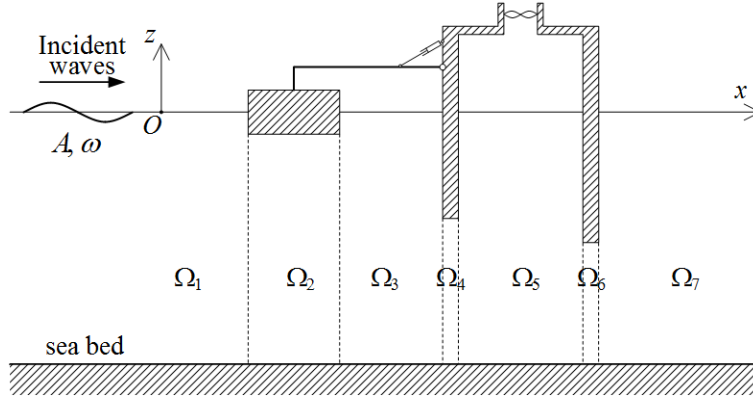
3 Expression of Φ_1 , the dominate equation and the boundary conditions that Φ_D and $\Phi_R^{(L)}$ ($L=1, 2,$
 4 3) should satisfy can all be found in our previous paper (Zheng and Zhang, 2016). Compared with
 5 $\Phi_R^{(L)}$ ($L=1, 2, 3$), due to the existence of air pressure oscillation inside the OWC chamber, the only
 6 different boundary condition for $\Phi_R^{(4)}$ happens on the free water surface in the OWC chamber,
 7 where $\Phi_R^{(4)}$ should satisfy

$$8 \quad \frac{\partial \Phi_R^{(4)}}{\partial z} - \frac{\omega^2}{g} \Phi_R^{(4)} = \frac{i\omega}{\rho g}, \quad (2)$$

9 in which ρ is the water density and g is the gravity acceleration.

10 2.2. Formulation of the wave diffraction/radiation problem

11 To solve the wave diffraction and radiation problems, the fluid domain is divided into 7
 12 subdomains denoted as Ω_j ($j=1, 2, \dots, 7$) as shown in Fig. 2.



13
 14 Fig. 2 Sketch of the subdomains of water domain

15 Utilizing the method of separation of variables, the analytical expressions for unknown
 16 diffracted/radiated spatial potential in each subdomain can be obtained as follows (Zheng and
 17 Zhang, 2016; Falnes, 2002):

18 Wave diffraction problem

19 In regions 1, $2m+1$, $2m$ and 7, the diffracted potentials may be expressed, respectively, as
 20 follows:

$$21 \quad \Phi_{D,1} = \sum_{j=1}^{\infty} A_{1,j}^D e^{\lambda_j x} Z_j(z) \quad \text{in } \Omega_1. \quad (3)$$

1 For $m=1, 2$,

$$2 \quad \Phi_{D,2m+1} = \sum_{j=1}^{\infty} \left(A_{2m+1,j}^D e^{\lambda_j x} + B_{2m+1,j}^D e^{-\lambda_j x} \right) Z_j(z) \text{ in } \Omega_{2m+1}. \quad (4)$$

3 For $m=1, 2, 3$,

$$4 \quad \Phi_{D,2m} = -\Phi_1 + A_{2m,1}^D x + B_{2m,1}^D + \sum_{j=2}^{\infty} \left(A_{2m,j}^D e^{\beta_{m,j} x} + B_{2m,j}^D e^{-\beta_{m,j} x} \right) \cos[\beta_{m,j}(z+h)] \text{ in } \Omega_{2m}. \quad (5)$$

$$5 \quad \Phi_{D,7} = \sum_{j=1}^{\infty} A_{7,j}^D e^{-\lambda_j x} Z_j(z) \text{ in } \Omega_7. \quad (6)$$

6 $A_{1,j}^D, A_{2m+1,j}^D, B_{2m+1,j}^D, A_{2m,j}^D, B_{2m,j}^D$ and $A_{7,j}^D$ as given in Eqs. (3)~(6) are unknown coefficients to
 7 be determined; Eq. (4) represents a general wave solution for the velocity potential in a uniform
 8 fluid of constant depth (Falnes, 2002); $\beta_{m,j}$ and λ_j are the eigenvalues of the j -th wave modes in
 9 subdomain 2m, and subdomains 1 and 2, respectively, given as:

$$10 \quad \lambda_1 = -ik, \quad j=1, \quad (7)$$

$$11 \quad \omega^2 = -\lambda_j g \tan(\lambda_j h), \quad j=2, 3, 4, \dots, \quad (8)$$

$$12 \quad \beta_{m,j} = \frac{(j-1)\pi}{h-d_m}, \quad j=2, 3, 4, \dots, \quad (9)$$

$$13 \quad Z_j(z) = N_j^{-0.5} \cos[\lambda_j(h+z)], \quad N_j = \frac{1}{2} \left[1 + \frac{\sin(2\lambda_j h)}{2\lambda_j h} \right], \quad (10)$$

14 in which k is the wave number satisfying $\omega^2 = gk \tanh(kh)$.

15 Wave radiation problem

16 In regions 1, 2m+1, 2m and 7, the radiated potentials can be expressed, respectively, as follows:

$$17 \quad \Phi_{R,1}^{(L)} = \sum_{j=1}^{\infty} A_{1,j}^{(L)} e^{\lambda_j x} Z_j(z) \text{ in } \Omega_1. \quad (11)$$

18 For $m=1,2$,

$$19 \quad \Phi_{R,2m+1}^{(L)} = \sum_{j=1}^{\infty} \left(A_{2m+1,j}^{(L)} e^{\lambda_j x} + B_{2m+1,j}^{(L)} e^{-\lambda_j x} \right) Z_j(z) - \frac{i\delta_{L,4}\delta_{m,2}}{\rho\omega} \text{ in } \Omega_{2m+1}. \quad (12)$$

20 For $m=1, 2, 3$,

$$1 \quad \Phi_{R,2m}^{(L)} = \Phi_{R,2m}^{p,L} + A_{2m,1}^{(L)}x + B_{2m,1}^{(L)} + \sum_{j=2}^{\infty} \left(A_{2m,j}^{(L)} e^{\beta_{m,j}x} + B_{2m,j}^{(L)} e^{-\beta_{m,j}x} \right) \cos \left[\beta_{m,j} (z+h) \right] \text{ in } \Omega_{2m}. \quad (13)$$

$$2 \quad \Phi_{R,7}^{(L)} = \sum_{j=1}^{\infty} A_{7,j}^{(L)} e^{-\lambda_j x} Z_j(z) \text{ in } \Omega_7. \quad (14)$$

3 In Eqs.(7)~(10), $A_{1,j}^{(L)}$, $A_{2m+1,j}^{(L)}$, $B_{2m+1,j}^{(L)}$, $A_{2m,j}^{(L)}$, $B_{2m,j}^{(L)}$ and $A_{7,j}^{(L)}$ are unknown coefficients to be
4 determined; $\delta_{i,j}$ denotes the Kronecker delta, and $\Phi_{R,2m}^{p,L}$ represents a special solution of $\Phi_{R,2m}^{(L)}$
5 expressed as

$$6 \quad \Phi_{R,2m}^{p,L} = \delta_{m,1} \left[\frac{(z+h)^2 - x^2}{2(h-d_m)} \delta_{2,L} - \frac{(z+h)^2(x-x_0) - \frac{1}{3}(x-x_0)^3}{2(h-d_m)} \delta_{3,L} \right]. \quad (15)$$

7 2.3. Solution to diffracted/radiated potentials

8 At either the interface between two adjacent subdomains or the fluid-structure interface, the
9 motions of the structures and fluids is fully coupled by pressures or/and velocities normal to the
10 interfaces. The continuity conditions at these interfaces for Φ_D has been previously given in
11 Zheng and Zhang (2016). To shorten the paper length, here only the continuity conditions for
12 $\Phi_R^{(L)}$ ($L=1, 2, 3, 4$) are presented as follows:

$$13 \quad \frac{\partial \Phi_{R,2m-1}^{(L)}}{\partial x} = \begin{cases} \delta_{m,1} [\delta_{1,L} + (z-z_0)\delta_{3,L}] & (x = x_{L,m}, \quad -d_m < z < 0) \\ \frac{\partial \Phi_{R,2m}^{(L)}}{\partial x} & (x = x_{L,m}, \quad -h < z < -d_m) \end{cases}, \quad (16)$$

$$14 \quad \frac{\partial \Phi_{R,2m+1}^{(L)}}{\partial x} = \begin{cases} \delta_{m,1} [\delta_{1,L} + (z-z_0)\delta_{3,L}] & (x = x_{R,m}, \quad -d_m < z < 0) \\ \frac{\partial \Phi_{R,2m}^{(L)}}{\partial x} & (x = x_{R,m}, \quad -h < z < -d_m) \end{cases}, \quad (17)$$

$$15 \quad \Phi_{R,2m-1}^{(L)} = \Phi_{R,2m}^{(L)} \quad (x = x_{L,m}, \quad -h < z < -d_m), \quad (18)$$

$$16 \quad \Phi_{R,2m}^{(L)} = \Phi_{R,2m+1}^{(L)} \quad (x = x_{R,m}, \quad -h < z < -d_m), \quad (19)$$

17 where $x_{L,m}$ and $x_{R,m}$ represent the horizontal positions of the left and right edges of subdomain
18 Ω_{2m} , respectively.

1 Upon substituting Eqs (3–6) for Φ_D in different subdomains into the continuity conditions for
 2 wave diffraction and Eqs.(11-14) for $\Phi_R^{(L)}$ in different subdomains into Eqs.(16-19), utilizing the
 3 orthogonality relations of the integration of eigen-functions over the vertical dimension (Zheng
 4 and Zhang, 2016) and taking the first M terms in the infinite series, a linear system of $12M$
 5 complex equations for either Φ_D or $\Phi_R^{(L)}$ with the same number of unknown coefficients are
 6 obtained. The unknown coefficients can be easily evaluated by solving a $12M$ -order linear matrix
 7 equation.

8 2.4. Hydrodynamic coefficients due to wave diffraction/radiation

9 2.4.1 Direct Method (DM) for solving hydrodynamic coefficients

10 wave diffraction

11 For fixed structures, the hydrodynamic forces acting on them called wave excitation forces are
 12 induced by both the undisturbed incident wave and the diffracted wave. The wave excitation
 13 force loading on the float in mode L ($L=1, 2, 3$) can be written as $\text{Re}\left(F_e^{(L)}e^{-i\omega t}\right)$, in which from
 14 the view of the definition of “wave excitation force”, $F_e^{(L)}$ is expressed as

$$15 \quad F_e^{(L)} = -i\omega\rho \int_{S_1} (\Phi_I + \Phi_D) n_L ds, \quad (20)$$

16 where S_1 is the wetted surface of the float; n_L is the component in mode L of the generalized
 17 normal vector.

18 Similarly, the upward flux at the water surface inside the OWC chamber due to the contributions
 19 of undisturbed incident wave and the diffracted wave, so-called the excitation volume flow, can
 20 be written as

$$21 \quad F_e^{(4)} = \int_{x_{R,2}}^{x_{L,3}} \frac{\partial(\Phi_I + \Phi_D)}{\partial z} \Big|_{z=0} dx. \quad (21)$$

22 wave radiation

23 Radiation force acting on the float in mode i ($i=1, 2, 3$) can be treated as one that is induced by
 24 the oscillations of both the float and the OWC written as $\text{Re}\left(F_R^{(i)}e^{-i\omega t}\right)$, in which

$$25 \quad \begin{aligned} F_R^{(i)} &= -i\omega\rho \int_{S_1} \left(\sum_{L=1}^3 \dot{A}_L \Phi_R^{(L)} + p \Phi_R^{(4)} \right) n_i ds \\ &= -i\omega\rho \int_{S_1} \sum_{L=1}^4 \dot{A}_L \Phi_R^{(L)} n_i ds = \sum_{L=1}^4 \dot{A}_L (i\omega a_{i,L} - c_{i,L}) \end{aligned}, \quad (22)$$

26 where $\dot{A}_4 = p$, $a_{i,L} = -\rho \int_{S_1} \text{Re}\left(\Phi_R^{(L)}\right) n_i ds$, and $c_{i,L} = -\rho\omega \int_{S_1} \text{Im}\left(\Phi_R^{(L)}\right) n_i ds$.

1 Similarly, the upward flux at the water surface inside the OWC chamber due to the radiated
 2 waves induced by the oscillations of both the float and the OWC can be written as

$$\begin{aligned}
 F_R^{(4)} &= \int_{x_{R,2}}^{x_{L,3}} \frac{\partial \sum_{L=1}^4 \dot{A}_L \Phi_R^{(L)}}{\partial z} \Big|_{z=0} dx \\
 &= \frac{\omega^2}{g} \sum_{L=1}^4 \dot{A}_L \sum_{j=1}^{\infty} \int_{x_{R,2}}^{x_{L,3}} \left(A_{5,j}^{(L)} e^{\lambda_j x} + B_{5,j}^{(L)} e^{-\lambda_j x} \right) Z_j(0) dx \\
 &= \frac{\omega^2}{g} \sum_{L=1}^4 \dot{A}_L \sum_{j=1}^{\infty} \frac{\left[A_{5,j}^{(L)} \left(e^{\lambda_j x_{L,3}} - e^{\lambda_j x_{R,2}} \right) - B_{5,j}^{(L)} \left(e^{-\lambda_j x_{L,3}} - e^{-\lambda_j x_{R,2}} \right) \right] Z_j(0)}{\lambda_j}, \\
 &= \sum_{L=1}^4 \dot{A}_L \left(i\omega a_{4,L} - c_{4,L} \right)
 \end{aligned} \tag{23}$$

4 in which

$$a_{4,L} = \frac{\omega}{g} \operatorname{Im} \left(\sum_{j=1}^{\infty} \frac{\left[A_{5,j}^{(L)} \left(e^{\lambda_j x_{L,3}} - e^{\lambda_j x_{R,2}} \right) - B_{5,j}^{(L)} \left(e^{-\lambda_j x_{L,3}} - e^{-\lambda_j x_{R,2}} \right) \right] Z_j(0)}{\lambda_j} \right), \tag{24}$$

$$c_{4,L} = -\frac{\omega^2}{g} \operatorname{Re} \left(\sum_{j=1}^{\infty} \frac{\left[A_{5,j}^{(L)} \left(e^{\lambda_j x_{L,3}} - e^{\lambda_j x_{R,2}} \right) - B_{5,j}^{(L)} \left(e^{-\lambda_j x_{L,3}} - e^{-\lambda_j x_{R,2}} \right) \right] Z_j(0)}{\lambda_j} \right). \tag{25}$$

7 Therefore, $F_R^{(i)} = \sum_{L=1}^4 \dot{A}_L \left(i\omega a_{i,L} - c_{i,L} \right)$ is valid for $i=1, 2, 3, 4$.

8 2.4.2 Indirect method for solving hydrodynamic coefficients 9 wave diffraction

10 In fact, apart from using the direct method as mentioned in Section 2.4.1, the generalized
 11 excitation forces may also be expressed in terms of the radiated wave's far-field coefficients
 12 using the Haskind Relation (HR). The excitation force (or the excitation volume flow) acting on a
 13 body (or an OWC) that experiences a plane wave propagating from a certain direction is related
 14 to the body's (or the OWC's) ability to radiate a wave into just that direction (Falnes, 2002). The
 15 generalized wave excitation force after using the HR can be derived as:

$$F_e^{(L)} = \frac{-2i\rho g A k h A_{1,1}^{(L)} (-1)^{\delta_{4,L}}}{Z_1(0)}, \tag{26}$$

17 Detail derivation of Eq.(26) is given in Appendix A.

1 wave radiation

2 Similar to the expression of the generalized excitation forces using the Haskind Relation,
 3 reciprocity relations exist for the radiation damping matrix (Falnes, 2002). By using the
 4 reciprocity relations, some of the wave radiation damping and added mass can be written in terms
 5 of the radiated wave's Far-Field Coefficients (FFC) as follows:

$$6 \quad c_{i,L} = \omega \rho k h \left(A_{7,1}^{(i)*} A_{7,1}^{(L)} + A_{1,1}^{(i)*} A_{1,1}^{(L)} \right) \quad (i = 1, 2, 3; L = 1, 2, 3), (i = L = 4), \quad (27)$$

$$7 \quad \mu_{i,L} = i \rho k h \left(A_{7,1}^{(i)*} A_{7,1}^{(L)} + A_{1,1}^{(i)*} A_{1,1}^{(L)} \right) \quad (i = 1, 2, 3; L = 4), (i = 4; L = 1, 2, 3), \quad (28)$$

8 where the superscript * denotes complex-conjugate.

9 2.5. Power absorption of the hybrid WEC

10 After solving the wave diffraction/radiation problem and obtaining the hydrodynamic
 11 coefficients, the response of the hybrid WEC in frequency domain can be calculated using the
 12 following dynamic motion equation:

$$13 \quad \begin{bmatrix} -i\omega(\mathbf{M} + \mathbf{M}_a + \mathbf{M}_{\text{PTO}}) + (\mathbf{C}_d + \mathbf{C}_{\text{PTO}}) + i\mathbf{K}_s/\omega & \mathbf{A}_J^T \\ \mathbf{A}_J & \mathbf{0} \end{bmatrix} \begin{Bmatrix} \dot{\mathbf{X}} \\ \mathbf{F}_J \end{Bmatrix} = \begin{Bmatrix} \mathbf{F}_c \\ \mathbf{0} \end{Bmatrix}, \quad (29)$$

14 where \mathbf{M} is the mass matrix; \mathbf{M}_a and \mathbf{C}_d are the added mass matrix and radiation damping matrix,
 15 respectively; \mathbf{M}_{PTO} and \mathbf{C}_{PTO} are the mass matrix and damping matrix, respectively, induced by
 16 the PTO system; \mathbf{K}_s is the hydrostatic restoring matrix; \mathbf{A}_J is the constraint matrix due to the
 17 hinge restriction to the float; the superscript T denotes transpose; $\dot{\mathbf{X}} = [\dot{A}_1 \quad \dot{A}_2 \quad \dot{A}_3 \quad \dot{A}_4]^T$
 18 represents the velocity response vector of the hybrid WEC to be determined; \mathbf{F}_J denotes the hinge
 19 force vector; \mathbf{F}_c is the generalized wave excitation force vector.

$$20 \quad \mathbf{A}_J = \begin{bmatrix} 1 & 0 & d & 0 \\ 0 & 1 & -D & 0 \end{bmatrix}, \mathbf{M} = \begin{bmatrix} m & & & \\ & m & & \\ & & I & \\ & & & 0 \end{bmatrix}, \mathbf{K}_s = \rho g \begin{bmatrix} 0 & & & \\ & a_1 & & \\ & & \frac{a_1^3}{12} - \frac{a_1 d_1^2}{2} & \\ & & & 0 \end{bmatrix},$$

$$21 \quad \mathbf{C}_{\text{PTO}} = \begin{bmatrix} 0 & & & \\ & 0 & & \\ & & c_1 & \\ & & & c_2 \end{bmatrix}, \mathbf{M}_{\text{PTO}} = \begin{bmatrix} 0 & & & \\ & 0 & & \\ & & 0 & \\ & & & \frac{V_0}{c_a^2 \rho_0} \end{bmatrix}, \quad (30)$$

22 in which m is the mass of the float; I is the rotary inertia of the float relative to the centre of mass;
 23 c_1 and c_2 represent the linear damping of the hydraulic cylinder and the OWC turbine PTO
 24 system, respectively; V_0 is the air chamber volume; c_a is the sound velocity in air; ρ_0 is the static

1 air density. In subsequent computations, $\rho/\rho_0=800$, $c_a=340\text{m/s}$ and the air chamber volume is
 2 $V_0=2a^2$ unless otherwise specified.

3 Wave power is absorbed by the damping in both the float PTO system and the OWC PTO system.
 4 After solving Eq.(29), $\dot{\mathbf{X}}$ is obtained and the average power that the hybrid WEC captures from
 5 regular waves can be written as

$$6 \quad P = \frac{1}{2} \left(c_1 |\dot{A}_3|^2 + c_2 |\dot{A}_4|^2 \right). \quad (31)$$

7 The power absorption efficiency is calculated as:

$$8 \quad \eta = \frac{P}{0.5 \rho g A^2 c_g}, \quad (32)$$

$$9 \quad \text{where } c_g = \frac{\omega}{2k} \left[1 + \frac{2kh}{\sinh(2kh)} \right].$$

10 2.6. Optimization of power absorption

11 The power absorption capability of a WEC is a particular subject of interest. As described above,
 12 although surge, heave and pitch modes of the float are all included in the float motion, only the
 13 pitch motion, together with the oscillation of water column, are used to drive PTO systems.
 14 Thanks to the mechanical relation between the surge, heave and pitch modes of the float induced
 15 by the hinge constraints, Eq. (29) can be reduced to the solution of a 2-order algebraic matrix
 16 equation with the employment of matrix blocking method as follows.

17 Matrix $[-i\omega(\mathbf{M} + \mathbf{M}_a + \mathbf{M}_{\text{PTO}}) + (\mathbf{C}_d + \mathbf{C}_{\text{PTO}}) + i\mathbf{K}_s/\omega]$ can be partitioned into four blocks \mathbf{S}_{11} ,
 18 \mathbf{S}_{12} , \mathbf{S}_{21} , and \mathbf{S}_{22} whose sizes are all 2×2 . The hinge force vector \mathbf{F}_J can be expressed in terms of
 19 wave excitation forces loading on the float in surge and heave modes, and the velocity response
 20 of both the float in pitch mode and the air pressure inside the chamber as

$$21 \quad \mathbf{F}_J = \begin{Bmatrix} F_e^{(1)} \\ F_e^{(2)} \end{Bmatrix} - [\mathbf{S}_{11} \quad \mathbf{S}_{12}] \begin{bmatrix} \mathbf{A}_T \\ \mathbf{I} \end{bmatrix} \begin{Bmatrix} \dot{A}_3 \\ \dot{A}_4 \end{Bmatrix} = \begin{Bmatrix} F_e^{(1)} \\ F_e^{(2)} \end{Bmatrix} - (\mathbf{S}_{11}\mathbf{A}_T + \mathbf{S}_{12}) \begin{Bmatrix} \dot{A}_3 \\ \dot{A}_4 \end{Bmatrix}, \quad (33)$$

$$22 \quad \text{where } \mathbf{A}_T = \begin{bmatrix} -d & 0 \\ D & 0 \end{bmatrix}.$$

23 In addition, \mathbf{F}_J , \dot{A}_3 , \dot{A}_4 , $F_e^{(3)}$ and $F_e^{(4)}$ should also satisfy the following relation:

$$24 \quad [\mathbf{S}_{21} \quad \mathbf{S}_{22}] \begin{bmatrix} \mathbf{A}_T \\ \mathbf{I} \end{bmatrix} \begin{Bmatrix} \dot{A}_3 \\ \dot{A}_4 \end{Bmatrix} - \mathbf{A}_T^T \mathbf{F}_J = (\mathbf{S}_{21}\mathbf{A}_T + \mathbf{S}_{22}) \begin{Bmatrix} \dot{A}_3 \\ \dot{A}_4 \end{Bmatrix} - \mathbf{A}_T^T \mathbf{F}_J = \begin{Bmatrix} F_e^{(3)} \\ F_e^{(4)} \end{Bmatrix}. \quad (34)$$

1 Submitting Eqs. (33-34) into Eq. (29) and making some rearrangements gives

$$2 \quad \left(\mathbf{A}_T^T \mathbf{S}_{11} \mathbf{A}_T + \mathbf{A}_T^T \mathbf{S}_{12} + \mathbf{S}_{21} \mathbf{A}_T + \mathbf{S}_{22} \right) \begin{Bmatrix} \dot{A}_3 \\ \dot{A}_4 \end{Bmatrix} = \begin{Bmatrix} F_e^{(3)} \\ F_e^{(4)} \end{Bmatrix} + \mathbf{A}_T^T \begin{Bmatrix} F_e^{(1)} \\ F_e^{(2)} \end{Bmatrix}, \quad (35)$$

3 in which the PTO damping coefficients (c_1 and c_2) can be easily separated, and Eq. (35) can be
4 rewritten into a 2-order linear matrix equation:

$$5 \quad \begin{bmatrix} A_0 + c_1 & B_0 \\ C_0 & D_0 + c_2 \end{bmatrix} \begin{Bmatrix} \dot{A}_3 \\ \dot{A}_4 \end{Bmatrix} = \begin{Bmatrix} E_0 \\ F_0 \end{Bmatrix}, \quad (36)$$

6 where the subscript “0” of $A_0 \sim F_0$ means that these parameters are independent of c_1 and c_2 .

7 After expressing \dot{A}_3 and \dot{A}_4 in terms of $A_0 \sim F_0$, c_1 and c_2 , and submitting them into Eq. (31), we
8 have the new expression of P as a two variable explicit function

$$9 \quad P(c_1, c_2) = \frac{1}{2} \frac{c_1 (u_1 c_2^2 + u_2 c_2 + u_3) + c_2 (u_4 c_1^2 + u_5 c_1 + u_6)}{c_1^2 c_2^2 + u_7 c_1^2 c_2 + u_8 c_1 c_2^2 + u_9 c_1^2 + u_{10} c_2^2 + u_{11} c_1 c_2 + u_{12} c_1 + u_{13} c_2 + u_{14}}, \quad (37)$$

10 where $u_1 \sim u_{14}$ are expressed in terms of $A_0 \sim F_0$: $u_1 = |E_0|^2$, $u_2 = 2 \operatorname{Re}[E_0^* (D_0 E_0 - B_0 F_0)]$,
11 $u_3 = |D_0 E_0 - B_0 F_0|^2$, $u_4 = |F_0|^2$, $u_5 = 2 \operatorname{Re}[F_0^* (A_0 F_0 - C_0 E_0)]$, $u_6 = |A_0 F_0 - C_0 E_0|^2$, $u_7 = 2 \operatorname{Re}(D_0)$,
12 $u_8 = 2 \operatorname{Re}(A_0)$, $u_9 = |D_0|^2$, $u_{10} = |A_0|^2$, $u_{11} = 2 \operatorname{Re}(A_0 D_0 - B_0 C_0 + A_0 D_0^*)$,
13 $u_{12} = 2 \operatorname{Re}[D_0^* (A_0 D_0 - B_0 C_0)]$, $u_{13} = 2 \operatorname{Re}[A_0^* (A_0 D_0 - B_0 C_0)]$, $u_{14} = |A_0 D_0 - B_0 C_0|^2$.

14 The frequency dependent maximum of absorbed power, denoted as $P_0(\omega)$, can be achieved
15 when $\partial P / \partial c_1 = 0$ and $\partial P / \partial c_2 = 0$. While for some rare cases, the maximum value of P may
16 occur at either c_1 or c_2 being 0 or $+\infty$.

17 For $c_2=0$, $P = \frac{1}{2} \frac{u_3 c_1}{u_9 c_1^2 + u_{12} c_1 + u_{14}}$ and the maximum absorbed power, denoted as P_1 , occurs if

$$18 \quad c_1 = \sqrt{u_{14}/u_9}, \text{ for which we have } P_1 = \frac{1}{2} \frac{u_3 \sqrt{u_{14}/u_9}}{2u_{14} + u_{12} \sqrt{u_{14}/u_9}};$$

19 For $c_1=0$, $P = \frac{1}{2} \frac{u_6 c_2}{u_{10} c_2^2 + u_{13} c_2 + u_{14}}$ and the maximum absorbed power, denoted as P_2 , occurs if

$$20 \quad c_2 = \sqrt{u_{14}/u_{10}}, \text{ for which we have } P_2 = \frac{1}{2} \frac{u_6 \sqrt{u_{14}/u_{10}}}{2u_{14} + u_{13} \sqrt{u_{14}/u_{10}}};$$

1 For $c_2=+\infty$, $P = \frac{1}{2} \frac{u_1 c_1}{c_1^2 + u_8 c_1 + u_{10}}$ and the maximum absorbed power, denoted as P_3 , occurs if

2 $c_1 = \sqrt{u_{10}}$, for which we have $P_3 = \frac{1}{2} \frac{u_1 \sqrt{u_{10}}}{2u_{10} + u_8 \sqrt{u_{10}}}$;

3 For $c_1=+\infty$, $P = \frac{1}{2} \frac{u_4 c_2}{c_2^2 + u_7 c_2 + u_9}$ and the maximum absorbed power, denoted as P_4 , occurs if

4 $c_2 = \sqrt{u_9}$, for which we have $P_4 = \frac{1}{2} \frac{u_4 \sqrt{u_9}}{2u_9 + u_7 \sqrt{u_9}}$.

5 In summary, the maximum absorbed power by the hybrid WEC, denoted as P_{\max} is

6
$$P_{\max} = \max(P_0, P_1, P_2, P_3, P_4). \quad (38)$$

7 The maximum power absorption efficiency for P_{\max} can be calculated in a similar way as given in
 8 Eq. (32), which is notated by η_{\max} . The corresponding optimized PTO damping for the float and
 9 the OWC are notated by $c_{\text{opt},1}$ and $c_{\text{opt},2}$, respectively.

10 2.7. Wave reflection and transmission coefficients

11 The spatial velocity potential in the distance far away from the hybrid WEC can be written as:

12
$$\Phi(-x_\infty, 0) = -\frac{\text{i}g}{\omega} \frac{Z_1(z)}{Z_1(0)} \left[A e^{-\text{i}kx_\infty} + \frac{\text{i}\omega}{g} Z_1(0) \left(A_{1,1}^{\text{D}} + \sum_{L=1}^4 \dot{A}^{(L)} A_{1,1}^{\text{R},L} \right) e^{\text{i}kx_\infty} \right], \quad (39)$$

13
$$\Phi(x_\infty, 0) = -\frac{\text{i}g}{\omega} \frac{Z_1(z)}{Z_1(0)} \left[A e^{\text{i}kx_\infty} + \frac{\text{i}\omega}{g} Z_1(0) \left(A_{7,1}^{\text{D}} + \sum_{L=1}^4 \dot{A}^{(L)} A_{7,1}^{\text{R},L} \right) e^{\text{i}kx_\infty} \right]. \quad (40)$$

14 Therefore, the wave reflection coefficient and the wave transmission coefficient of the WEC,
 15 denoted as R and T , respectively, can be calculated as:

16
$$R = \left| \frac{\omega}{gA} Z_0(0) \left(A_{1,1}^{\text{D}} + \sum_{L=1}^4 \dot{A}^{(L)} A_{1,1}^{\text{R},L} \right) \right|, \quad (41)$$

17
$$T = \left| 1 + \frac{\text{i}\omega}{gA} Z_0(0) \left(A_{7,1}^{\text{D}} + \sum_{L=1}^4 \dot{A}^{(L)} A_{7,1}^{\text{R},L} \right) \right|. \quad (42)$$

18 3. Model validation

19 To validate the solutions of wave diffraction and radiation problems in the analytical model as
 20 described in Section 2, wave excitation forces/volume flux, added mass and radiation damping
 21 are all evaluated by using both direct method and indirect method. By checking these results of

1 the certain hydrodynamic parameters using different methods, the solutions of wave diffraction
2 and radiation problems can be validated if good agreements are satisfied. What is more,
3 hydrodynamic performance of an OWC consisting of two vertical thin barriers with unequal
4 length is also evaluated and is compared with published results (Falnes and McIver, 1985). The
5 theoretical maximum power absorption of the hybrid WEC, wave reflection and transmission
6 coefficients can be validated by comparing with the results from trial-and-error method and by
7 checking the energy conservation identity, respectively.

8 The excitation forces/volume flux and hydrodynamic coefficients together with both float PTO
9 damping and OWC PTO damping are normalized as follows:

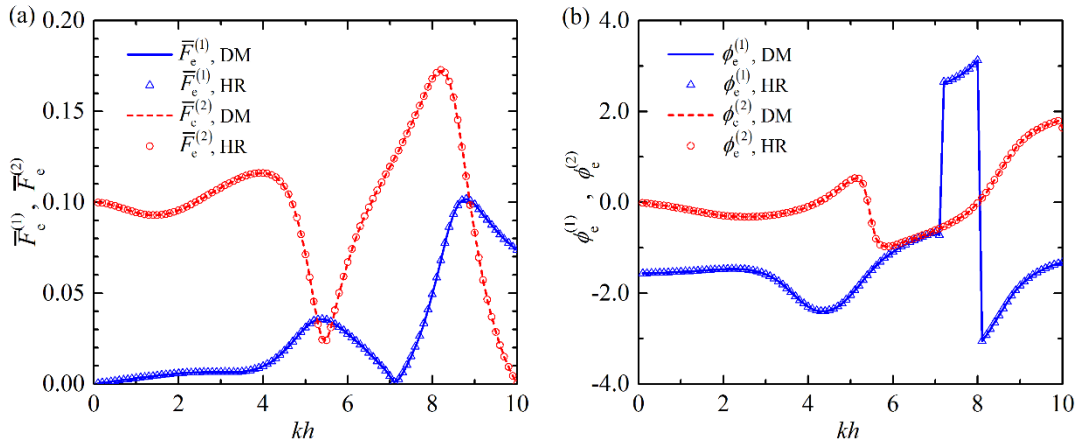
$$10 \quad \bar{F}_e^{(j)} = \begin{cases} \frac{|F_e^{(j)}|}{\rho g A h}, & j=1,2 \\ \frac{|F_e^{(j)}|}{\rho g A h^2}, & j=3 \\ \frac{|F_e^{(j)}|}{A \sqrt{g h}}, & j=4 \end{cases}, \quad \bar{c}_{i,j} = \begin{cases} \frac{c_{i,j}}{\rho h \sqrt{g h}}, & i=1,2; j=1,2 \\ \frac{c_{i,j}}{\rho h^2 \sqrt{g h}}, & (i=1,2; j=3), (i=3; j=1,2) \\ \frac{c_{i,j}}{h}, & (i=1,2; j=4), (i=4; j=1,2) \\ \frac{c_{i,j}}{\rho h^3 \sqrt{g h}}, & i=j=3 \\ \frac{c_{i,j}}{h^2}, & (i=3; j=4), (i=4; j=3) \\ \frac{\rho g c_{i,j}}{\sqrt{g h}}, & i=j=4 \end{cases},$$

$$11 \quad \bar{\mu}_{i,j} = \begin{cases} \frac{\omega \mu_{i,j}}{\rho h \sqrt{g h}}, & i=1,2; j=1,2 \\ \frac{\omega \mu_{i,j}}{\rho h^2 \sqrt{g h}}, & (i=1,2; j=3), (i=3; j=1,2) \\ \frac{\omega \mu_{i,j}}{h}, & (i=1,2; j=4), (i=4; j=1,2) \\ \frac{\omega \mu_{i,j}}{\rho h^3 \sqrt{g h}}, & i=j=3 \\ \frac{\omega \mu_{i,j}}{h^2}, & (i=3; j=4), (i=4; j=3) \\ \frac{\omega \rho g \mu_{i,j}}{\sqrt{g h}}, & i=j=4 \end{cases},$$

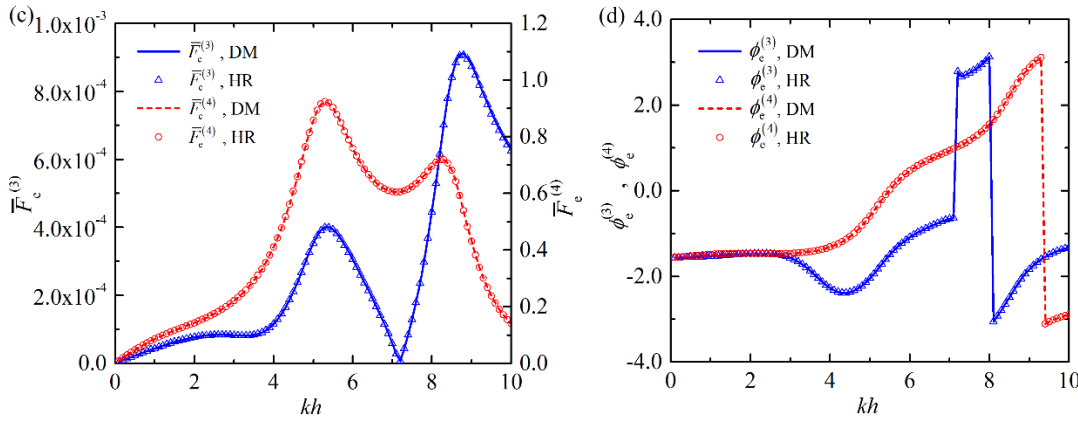
$$12 \quad \bar{\dot{x}} = \frac{\dot{x} \sqrt{g h}}{A g}, \quad \bar{p} = \frac{p}{\rho g A}, \quad \bar{c}_{\text{opt}}^{(1)} = \frac{c_{\text{opt},1}}{\rho h^3 \sqrt{g h}}, \quad \bar{c}_{\text{opt}}^{(2)} = \frac{\rho g c_{\text{opt},2}}{\sqrt{g h}}.$$

13 Figure 3 gives the results of wave excitation forces/volume flux for the hybrid WEC with
14 $a_1/h=0.1, a_2/h= a_3/h=0.005, d_1/h=0.025, d_2/h=0.1, d_3/h=0.15, D/h=0.15, a/h=0.1$. The
15 corresponding wave damping and added mass are illustrated in Figs. 4 and 5, respectively.

1

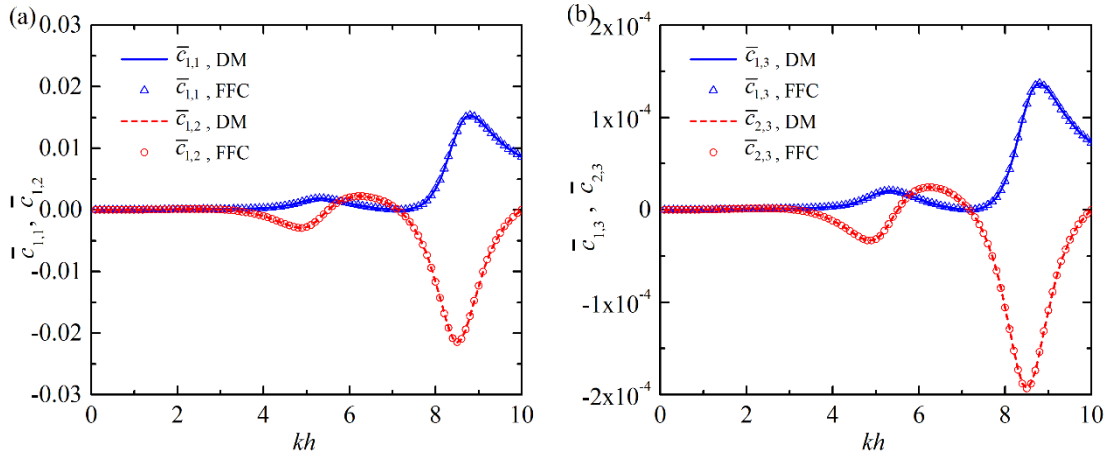


2

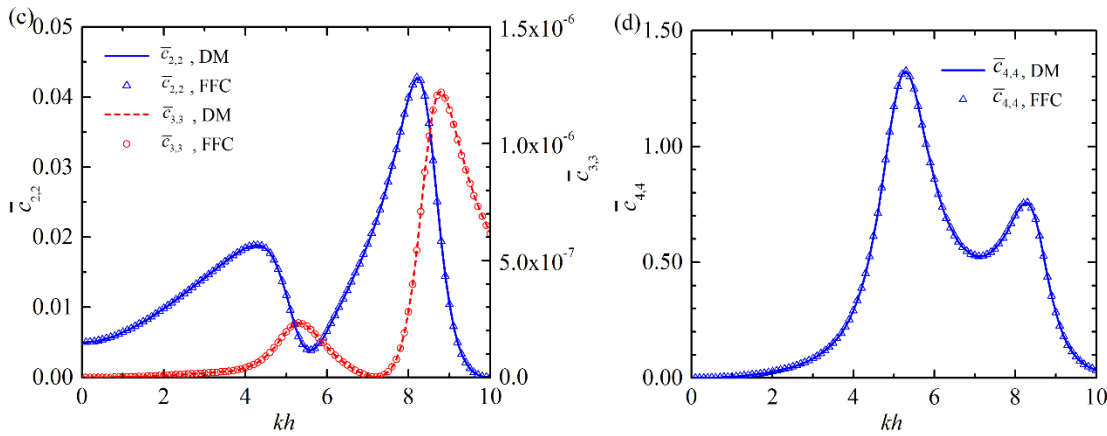


3

4 Fig. 3 Wave excitation forces/volume flux for $a_1/h=0.1$, $a_2/h= a_3/h=0.005$, $d_1/h=0.025$, $d_2/h=0.1$,
 5 $d_3/h=0.15$, $D/h=0.15$, $a/h=0.1$: (a) Dimensionless magnitudes of surge and heave wave excitation
 6 forces acting on the float; (b) Phases of surge and heave wave excitation forces acting on the
 7 float; (c) Dimensionless magnitudes of pitch wave excitation force acting on the float and wave
 8 excitation volume flux of the OWC; (d) Phases of pitch wave excitation force acting on the float
 9 and wave excitation volume flux of the OWC.

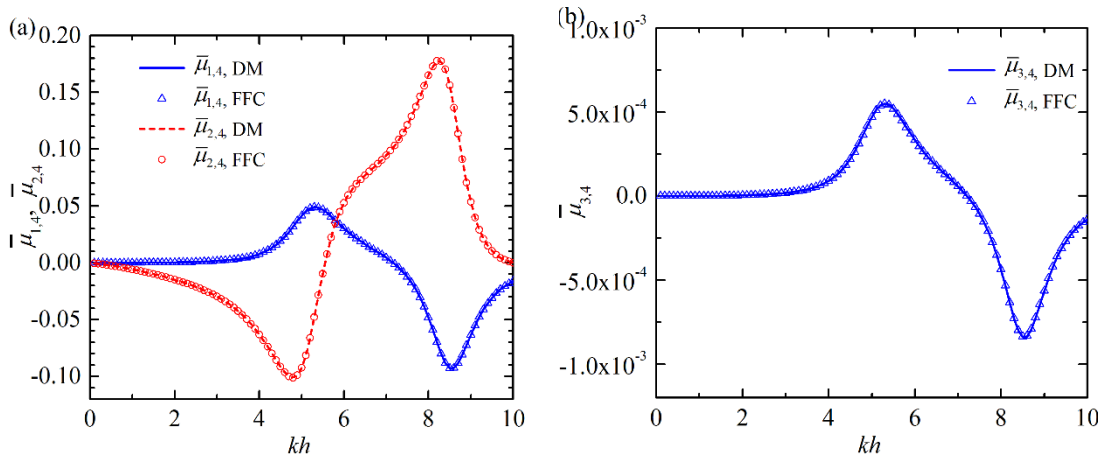


1



2

3 Fig. 4 Wave radiation damping for $a_1/h=0.1$, $a_2/h= a_3/h=0.005$, $d_1/h=0.025$, $d_2/h=0.1$, $d_3/h=0.15$,
 4 $D/h=0.15$, $a/h=0.1$: (a) Wave radiation damping of the float in surge mode due to the oscillation
 5 of the float in surge and heave modes; (b) Wave radiation damping of the float in surge and heave
 6 modes due to the oscillation of the float in pitch mode; (c) Wave radiation damping of the float in
 7 heave and pitch modes due to the oscillation of the float in heave and pitch modes, respectively;
 8 (d) Wave radiation damping of the OWC due to the air pressure oscillation inside the OWC
 9 chamber.

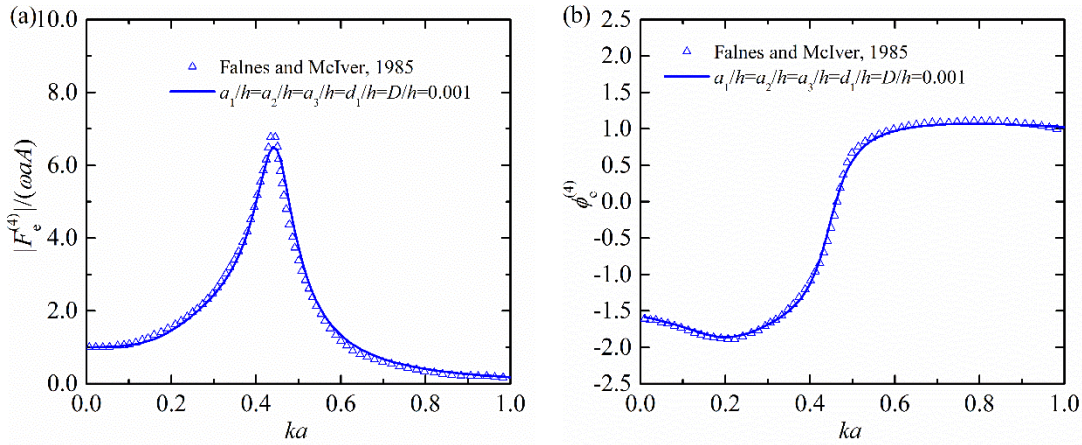


10

1 Fig. 5 Added mass for $a_1/h=0.1$, $a_2/h= a_3/h=0.005$, $d_1/h=0.025$, $d_2/h=0.1$, $d_3/h=0.15$, $D/h=0.15$,
 2 $a/h=0.1$: (a) Added mass of the float in surge and heave modes due to the air pressure oscillation
 3 inside the OWC chamber; (b) Added mass of the float in pitch mode due to the air pressure
 4 oscillation inside the OWC chamber.

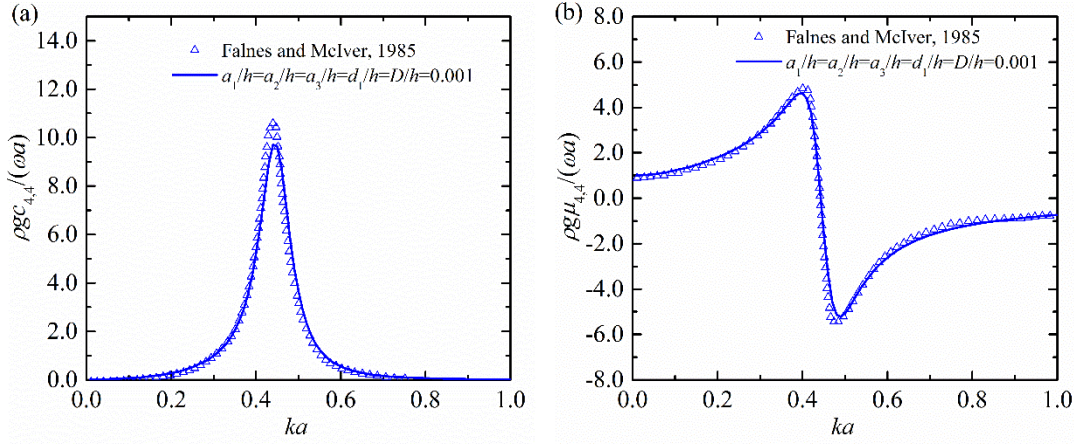
5 As shown in Figs. 3~5, results of the wave excitation forces/volume flux, wave damping and
 6 added mass of the hybrid WEC by using direct and indirect methods agree perfectly with each
 7 other.

8 Previously, Falnes and McIver (1985) used to study the power absorption by an OWC, which is
 9 composed of two vertical thin barriers with unequal length. Here, after setting the float width,
 10 float submergence depth and thickness of both fore wall and aft wall of OWC chamber to rather
 11 small values, the hybrid WEC looks rather similar with the device studied by Falnes and McIver
 12 (1985). The obtained results of wave excitation volume flux and the corresponding hydrodynamic
 13 coefficients for $a_1/h=a_2/h=a_3/h=0.001$, $d_1/h=0.001$, $d_2/h=0.15$, $d_3/h=0.25$, $D/h=0.001$, $a/h=0.1$ are
 14 compared with those from Falnes and McIver (1985) in Figs. 6 and 7.



15
 16 Fig. 6 Dimensionless excitation volume flux versus ka for the chosen geometrical parameters:
 17 $d_2/h=0.15$, $d_3/h=0.25$, $a/h=0.1$. (a) Amplitude; (b) Phase. (Normalizing principle adopted by
 18 Falnes and McIver (1985) is applied to the present figure)

19

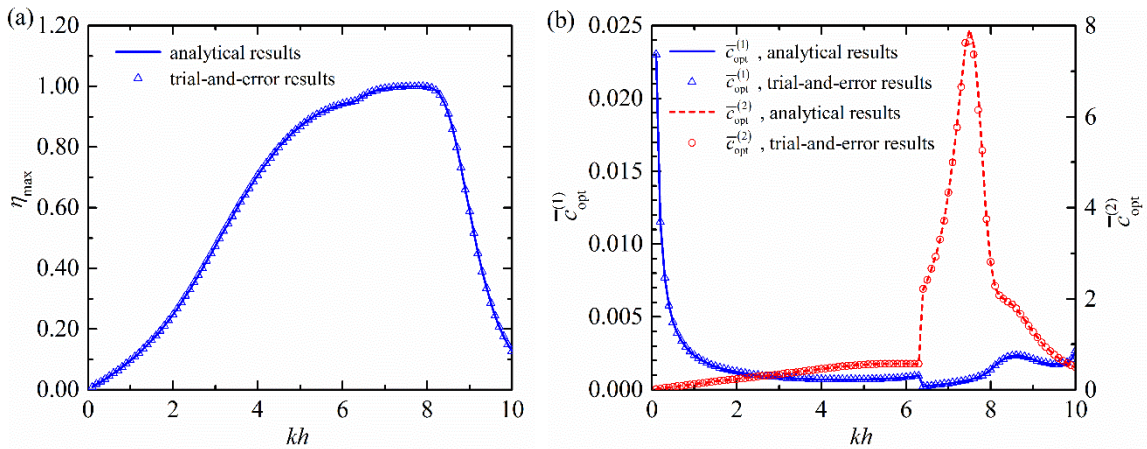


1

2 Fig. 7 Dimensionless radiation damping and added mass versus ka for the chosen geometrical
 3 parameters: $d_2/h=0.15$, $d_3/h=0.25$, $a/h=0.1$. (a) Radiation damping coefficient; (b) Added mass
 4 coefficient. (Normalizing principle adopted by Falnes and McIver (1985) is applied to the present
 5 figure)

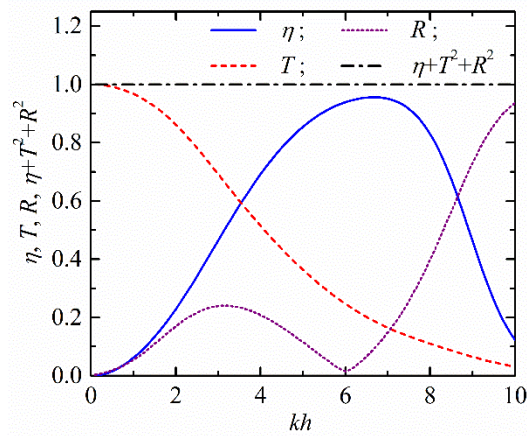
6 The good agreement between the obtained results and those from Falnes and McIver (1985) is
 7 also obtained as plotted in Figs. 6 and 7. It can be learnt from Figs. 3~7 that the present analytical
 8 model performs quite well in solving wave diffraction and radiation problems of the hybrid WEC.

9 Figure 8a illustrates the comparison between the analytical results of the maximum power
 10 absorption efficiency and the numerical ones using trial-and-error method for $a_1/h=0.1$, $a_2/h=$
 11 $a_3/h=0.005$, $d_1/h=0.025$, $d_2/h=0.1$, $d_3/h=0.15$, $D/h=0.15$, $a/h=0.1$, $d/h=0.05$. The trial-and-error
 12 method is adopted for searching the maximum efficiency in the frame of $\bar{c}^{(1)} \in [0, 0.025]$ and
 13 $\bar{c}^{(2)} \in [0, 8.0]$. The corresponding optimized float PTO damping and OWC PTO damping are
 14 also given in Fig.8b. Analytical and numerical results of η_{\max} , $\bar{c}_{\text{opt}}^{(1)}$ and $\bar{c}_{\text{opt}}^{(2)}$ are found to be in
 15 very good agreement for different wave conditions.



16

1 Fig.8 Variation of η_{\max} , $\bar{c}_{\text{opt}}^{(1)}$ and $\bar{c}_{\text{opt}}^{(2)}$ with kh for $a_1/h=0.1$, $a_2/h=$
2 $a_3/h=0.005$, $d_1/h=0.025$,
3 $d_2/h=0.1$, $d_3/h=0.15$, $D/h=0.15$, $a/h=0.1$, $d/h=0.05$: (a) η_{\max} ; (b) $\bar{c}_{\text{opt}}^{(1)}$ and $\bar{c}_{\text{opt}}^{(2)}$.
4 Figure 9 shows the results of η , R , T and $\eta + R^2 + T^2$ varying with kh for $a_1/h=0.1$, $a_2/h=$
5 $a_3/h=0.005$, $d_1/h=0.025$, $d_2/h=0.1$, $d_3/h=0.15$, $D/h=0.15$, $a/h=0.1$, $d/h=0.05$, $\bar{c}^{(1)}=0.001$ and $\bar{c}^{(2)}$
6 $=0.5$. The energy conservation relationship $\eta + R^2 + T^2=1$ is satisfied perfectly, which indirectly
7 validates the present analytical model as well.



8 Fig.9 Variation of η , R , T and $\eta + R^2 + T^2$ with kh for $a_1/h=0.1$, $a_2/h=$
9 $a_3/h=0.005$, $d_1/h=0.025$,
10 $d_2/h=0.1$, $d_3/h=0.15$, $D/h=0.15$, $a/h=0.1$, $d/h=0.05$, $\bar{c}^{(1)}=0.001$ and $\bar{c}^{(2)}=0.5$.

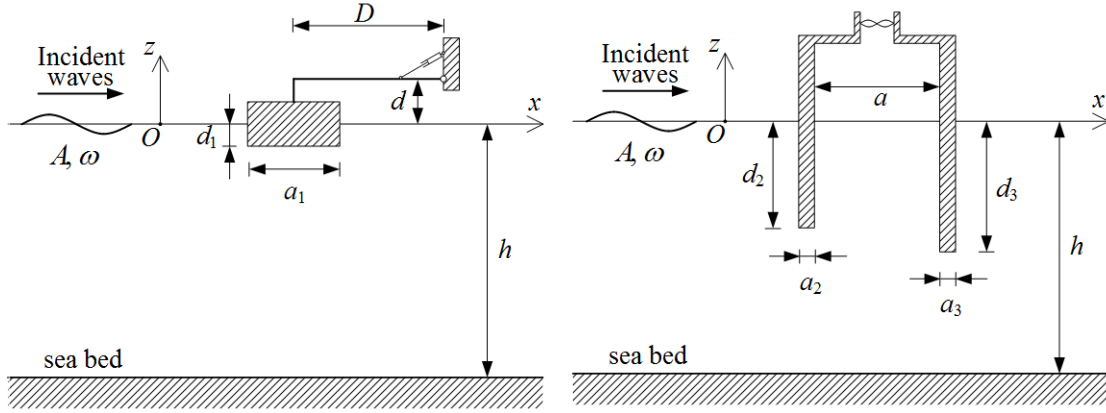
10 Although the hybrid WEC can be used as a kind of floating breakwaters by reducing amplitude of
11 the wave transmitted far behind the device, in the following sections, the study is mainly focused
12 on the performance in wave power exploitation.

13 4. Model Application

14 4.1. Comparison between the hybrid WEC and the isolated float and OWC

15 To study the influence of the hydrodynamic interaction between the float and the OWC on power
16 absorption of the hybrid WEC, the wave power absorbed by the isolated float and OWC working
17 in open sea, as show in Fig. 10, are also evaluated, respectively, as a comparison with that of the
18 hybrid WEC.

1



2

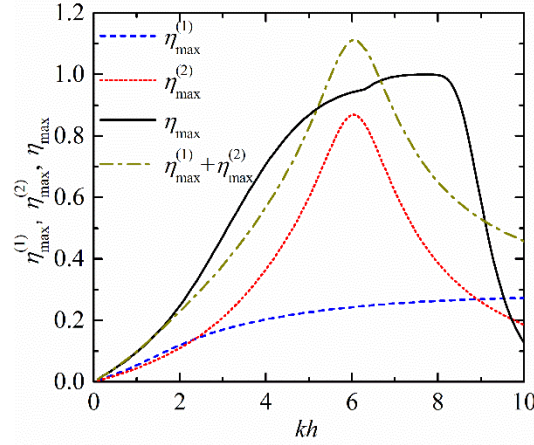
Fig. 10 Sketches of the isolated OWC and the isolated hinged float: (a) isolated float; (b) isolated OWC

3

4 The wave excitation forces and hydrodynamic coefficients of an isolated float (as shown in
 5 Fig.10a) can be evaluated using the analytical model proposed by Zheng et al. (2014). Analytical
 6 solution of wave diffraction and radiation by the isolated OWC (as shown in Fig.10b) can be
 7 derived base on the study carried out by Zheng and Zhang (2016). As both the oscillating motion
 8 of the isolated float and that of the isolated OWC can be treated as an oscillating system with only
 9 one degree of freedom, the maximized absorbed power and the corresponding optimal PTO
 10 damping for each situation can be calculated quite easily by solving a partial differential equation
 11 of single degree of freedom (Falnes, 2002).

12 Figure 11 illustrates the frequency response comparison of the maximum power capture
 13 efficiency of the hybrid WEC and those of the hinged float and the OWC when they are
 14 independently deployed for $a_1/h=0.1$, $a_2/h= a_3/h=0.005$, $d_1/h=0.025$, $d_2/h=0.1$, $d_3/h=0.15$,
 15 $D/h=0.15$, $a/h=0.1$, $d/h=0.05$. For $kh<10$, the maximum power capture efficiency of the hinged
 16 float, $\eta_{\max}^{(1)}$, is no more than 0.3. While as kh increases from 0 to 10, the maximum efficiency of
 17 the isolated OWC, $\eta_{\max}^{(2)}$, first increases and then decreases after reaching the peak value of 0.87 at
 18 $kh=6.0$ with a narrow bandwidth. $\eta_{\max}^{(2)}>0.8$ only occurs at $5.7<kh<6.4$. After combining these
 19 segments together, i.e., the hybrid WEC, the power extraction capacity is significantly improved.
 20 For $7.1<kh<8.0$, almost all the incident power can be captured when the PTO damping
 21 coefficients are optimized. What is better, the frequency bandwidth for $\eta_{\max}>0.8$ is $4.6<kh<8.7$,
 22 much wider than that of the isolated OWC. It is very interesting to find that if the hinged float in
 23 the absence of the OWC and the OWC in the absence of the hinged float are considered,
 24 respectively, the efficiency of both of them ($\eta_{\max}^{(1)} + \eta_{\max}^{(2)}$) is smaller than the efficiency of the
 25 hybrid WEC (η_{\max}) for $1.4<kh<5.1$ and $6.7<kh<9.0$, as shown in Fig.11. And the frequency
 26 bandwidth of η_{\max} of the hybrid WEC is larger than those of both the isolated hinged float and
 27 isolated OWC ($\eta_{\max}^{(1)} + \eta_{\max}^{(2)}$) for $\eta > 50\%$. This means that the hydrodynamic interaction between
 28 the float and the OWC plays a positive effect on both the power absorption for some range of

1 wave conditions and frequency response width of the hybrid WEC. Although the peak value of
 2 η_{\max} of the hybrid WEC is smaller than that of both the isolated hinged float and isolated OWC,
 3 it is believed that the hybrid WEC can be used to a wider range of wave conditions with a rather
 4 high power absorption efficiency. In the random waves with more incident power distributed at
 5 $1.4 < kh < 5.1$ and $6.7 < kh < 9.0$, output power of the hybrid WEC could be larger than the sum of
 6 output power of both the isolated hinged float and isolated OWC.



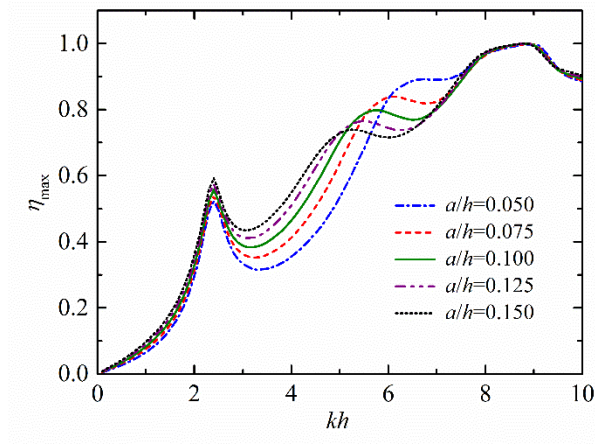
7

8 Fig. 11 Variation of η_{\max} , $\eta_{\max}^{(1)}$ and $\eta_{\max}^{(2)}$ with kh for $a_1/h=0.1$, $a_2/h= a_3/h=0.005$, $d_1/h=0.025$,
 9 $d_2/h=0.1$, $d_3/h=0.15$, $D/h=0.15$, $a/h=0.1$, $d/h=0.05$.

10 4.2. Impact analysis on power absorption by multiple parameters

11 4.2.1 Effect of OWC chamber width

12 Figure 12 shows the frequency response of η_{\max} for various OWC chamber widths (a/h). Due to
 13 the existence of the hinged float, the η_{\max} - kh curve of the hybrid WEC could hold more peaks
 14 with some specified structural dimensions (as given in Fig. 12), rather than merely one single
 15 peak for an isolated stationary offshore OWC (Elhanafi et al., 2017). For $kh < 5.0$, the larger a/h is,
 16 the larger η_{\max} by the hybrid WEC can be achieved whereas when $6.0 < kh < 6.5$ a/h shows the
 17 opposite effect on η_{\max} . It is noted that once a/h is doubled from 0.05 to 0.10, the maximum
 18 increase in η_{\max} can reach 40%. However, the influence of a/h on η_{\max} is not obvious for long
 19 wave length and short wave length, such as $kh < 2.5$ and $kh > 7.5$. As OWC chamber width (a/h)
 20 increases from 0.05 to 0.15, the value of kh , where the second peak of η_{\max} - kh curve occurs,
 21 decreases from 6.7 to 5.3.



1

2

Fig. 12 Variation of η_{\max} for various OWC chamber width (a/h) with $a_1/h=0.05$, $a_2/h=$

3

$a_3/h=0.005$, $d_1/h=0.05$, $d_2/h=0.1$, $d_3/h=0.15$, $D/h=0.1$, $d/h=0.1$.

4

4.2.2 Effect of submergence of the OWC side walls

5

The frequency response of η_{\max} for various submergences of the OWC fore wall (d_2/h) is plotted

6

in Fig. 13. It shows that, for $kh < 4.0$, a larger value of d_2/h is welcome for capturing power from

7

waves. This result is consistent with the corresponding numerical one for an offshore stationary

8

OWC, that the energy extraction in long waves can be improved with the increase of the

9

submergence of lips (Elhanafi et al., 2017). Compared to the other device with a larger d_2/h , the

10

hybrid WEC with the smallest d_2/h ($=0.05$) has the least power capture capacity for all the wave

11

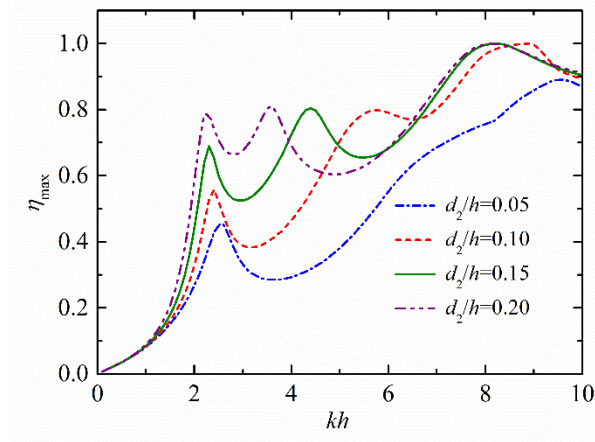
conditions studied ($kh < 10$). However, increasing d_2/h will not play a positive effect on power

12

absorption for all kh . For example, when $kh=5.8$, the corresponding η_{\max} is 0.8 for $d_2/h=0.10$,

13

which is obviously larger than those for $d_2/h=0.05$, 0.15, and 0.20.



14

15

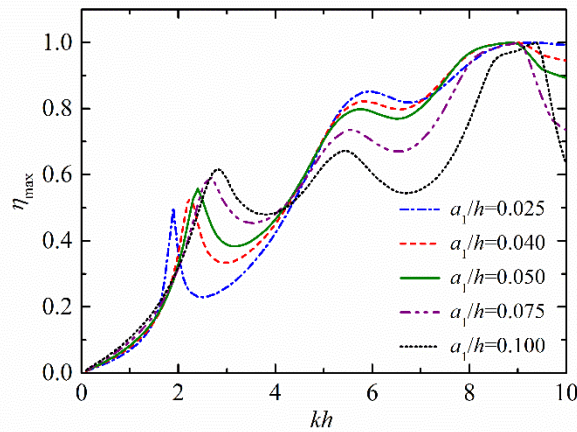
Fig. 13 Variation of η_{\max} for various submergence of the OWC side walls (d_2/h) with $a_1/h=0.05$,

16

$a_2/h= a_3/h=0.005$, $d_1/h=0.05$, $d_3/h=d_2/h+0.05$, $a/h=0.1$, $D/h=0.1$, $d/h=0.1$.

1 4.2.3 Effect of float width

2 As another vital parameter affecting power absorption of the hybrid WEC, influence of float
 3 width (a_1/h) is illustrated in Fig. 14. It can be learned that the first and second peaks of the η_{\max} -
 4 kh curve, occurring at $1.0 < kh < 4.0$ and $4.4 < kh < 7.2$, respectively, both are quite sensitive to a_1/h .
 5 The larger a_1/h is, the larger the first peak value of η_{\max} and the corresponding kh are, whereas
 6 the larger a_1/h is, the smaller the second peak value of η_{\max} and the corresponding kh are. While
 7 for $4.4 < kh < 7.2$, more power can be absorbed by the hybrid WEC with a smaller a_1/h . Thus,
 8 within $kh \in [1.0, 7.2]$ in which the water depth is specifically given, for waves with a smaller
 9 wave length (or high wave frequency) there is a demand to deploy a hybrid WEC device with a
 10 smaller a_1/h to realize more power absorption whereas for waves with a larger wave length there
 11 is a demand to deploy a hybrid WEC device generally with a larger a_1/h , which is mainly due to
 12 its larger peak value of power absorption efficiency and wider response width.



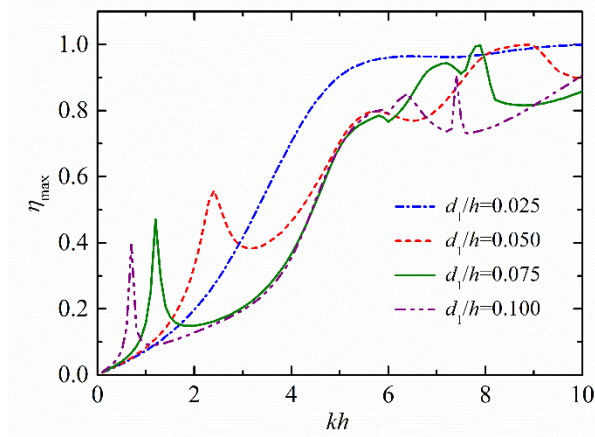
13

14 Fig. 14 Variation of η_{\max} for various float width (a_1/h) with $a_2/h = a_3/h = 0.005$, $d_1/h = 0.05$,
 15 $d_2/h = 0.1$, $d_3/h = 0.15$, $a/h = 0.1$, $D/h = 0.1$, $d/h = 0.1$.

16 4.3.4 Effect of float draft

17 Figure 15 shows the variation of η_{\max} with kh for various float draft (d_1/h) ranging from 0.025 to
 18 0.1. For $d_1/h = 0.025$, as kh increases from 0 to 10, η_{\max} first increases and then tends to be stable
 19 after reaching 0.95 at $kh = 5.4$. As a comparison, the η_{\max} - kh curves representing the rest cases
 20 with a larger d_1/h are quite different from that for $d_1/h = 0.025$. A sharp peak happens at $0 < kh < 3.0$
 21 for $d_1/h = 0.050$, 0.075 , and 0.100 , respectively. The hybrid WEC with a larger d_1/h means a
 22 smaller first resonant frequency of the float, therefore the sharp peak moves toward the left side
 23 of the kh axis. It can be seen that for waves with long wave length, there is a need of a larger d_1/h
 24 to match waves so as to acquire a larger η_{\max} , but this is at the expense of narrowing the
 25 frequency response width. Therefore, for waves with long wave length and a certain frequency
 26 width, even though the natural frequency of the device matches the waves to obtain the peak
 27 value of η_{\max} , the total power absorbed by the WEC is still quite limited due to a narrower
 28 frequency response bandwidth. It can be seen clearly that, for waves with short wave length (or

1 high wave frequency) and a certain frequency width, wave energy is converted efficiently, and
 2 the smaller the float draft (d_1/h) is, generally the larger the total power absorbed is.

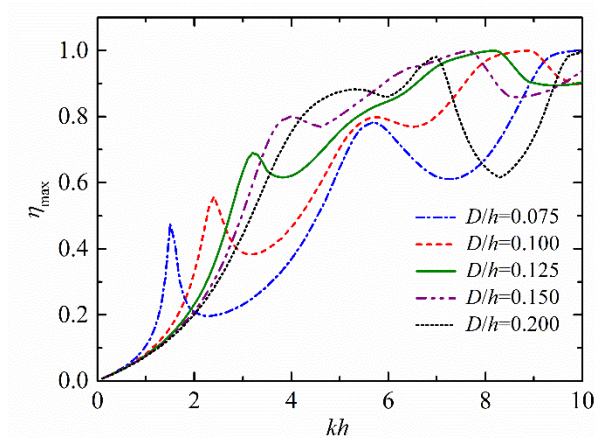


3

4 Fig. 15 Variation of η_{\max} for various float draft (d_1/h) with $a_1/h=0.05$, $a_2/h= a_3/h=0.005$,
 5 $d_2/h=0.1$, $d_3/h=0.15$, $a/h=0.1$, $D/h=0.1$, $d/h=0.1$.

6 4.3.5 Effect of the distance between float center and OWC

7 The distance between float center and OWC (D/h) plays an important role in affecting the
 8 hydrodynamic interaction between the float and the OWC. Effect of D/h on the maximum power
 9 absorption efficiency can be found in Fig. 16. As D/h increases from 0.075 to 0.2 with the step of
 10 0.025, the first peak value of η_{\max} - kh curve increases proportionally from 0.48 to 0.88, and its
 11 corresponding kh also increases from 1.5 to 5.3. Therefore, for a smaller wave frequency there is
 12 a demand to deploy a hybrid WEC with a smaller D/h in order to achieve the maximum power
 13 absorption efficiency. Conversely, a hybrid WEC with a larger D/h need be deployed. It has to be
 14 noted that the smaller D/h is, the smaller the frequency response bandwidth of the hybrid WEC is.

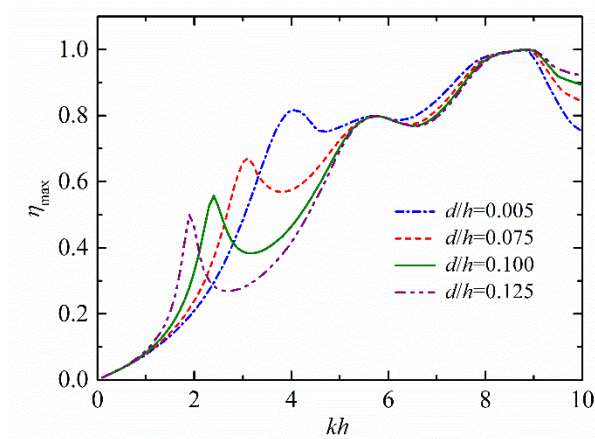


15

16 Fig. 16 Variation of η_{\max} for various distance between float center and OWC ($D/h=0.1$) with
 17 $a_1/h=0.05$, $a_2/h= a_3/h=0.005$, $d_1/h=0.05$, $d_2/h=0.1$, $d_3/h=0.15$, $a/h=0.1$, $d/h=0.1$.

1 4.3.6 Effect of vertical hinge position of the rigid arm

2 Although the vertical hinge position of the rigid arm (d/h) does not affect the basic hydrodynamic
3 coefficients of the hybrid WEC as calculated in the analytical model, it has a significant influence
4 on the rotary stiffness and inertia of the hinged float. Hence the motion response and power
5 absorption can also be changed by varying d/h , as shown in Fig. 17. As d/h increases from 0.005
6 to 0.125, the rotary inertia of the float relative to the hinge position increases as well, resulting in
7 a smaller resonant frequency together with a smaller first peak value of η_{\max} .



8

9 Fig. 17 Variation of η_{\max} for various vertical hinge position of the rigid arm (d/h) with
10 $a_1/h=0.05$, $a_2/h= a_3/h=0.005$, $d_1/h=0.05$, $d_2/h=0.1$, $d_3/h=0.15$, $a/h=0.1$, $D/h=0.1$.

11 5. Conclusions

12 We propose a hybrid WEC device consisting of a fixed inverted flume with long length and a
13 bottom hole, and a long floating cube hinged with the flume. An analytical model is developed
14 for the power extraction of the device based on linear potential flow theory and eigen-function
15 matching method in the two-dimensional Cartesian coordinate system.

16 The wave excitation forces/volume flux, added mass and wave damping are all calculated by the
17 analytical model using different approaches. Additionally, hydrodynamic performance of an
18 OWC consisting of two vertical thin barriers with unequal length is also evaluated and is
19 compared with published results (Falnes and McIver, 1985). The good agreement of these results
20 between each other shows that the present analytical model is correct. In addition, the analytical
21 results of the maximum power absorbed by the device is compared with those using trial-and-
22 error method. Energy conservation relationship is also checked to indirectly validate the present
23 analytical model.

24 The validated analytical model is then adopted to carry out the study on power capture capability
25 of the device with different geometrical dimension. For some specified dimensions, results are
26 also compared with a parallel study of an isolated OWC and an isolated float. Results reveal that:
27 the power extraction capacity can be significantly improved for a wide range of wave conditions
28 after combining the isolated OWC and the isolated float together. The hydrodynamic interaction

1 between the float and the OWC plays a positive effect on power absorption of the hybrid WEC
2 for some certain wave conditions.

3 It is found that the influence of device geometry on the power absorption can be significant and
4 varies considerably, depending on wave length. For $3.0 < kh < 4.0$, the hybrid WEC with a larger
5 water column width inside the OWC chamber, a larger submergence of the side walls of the
6 OWC chamber, a larger float width, while a smaller float draft is welcome in absorbing more
7 power from incident waves. As kh increase from 0 towards 5.0, there is generally a peak value of
8 $\eta_{\max} - kh$ curve, which turns larger for the hybrid WEC with a larger water column width inside
9 the OWC chamber, a larger submergence of the side walls of the OWC chamber, a larger float
10 width, a larger distance between the float center and the fore wall of OWC, a smaller float draft
11 and a smaller height of the hinge relative to the mean water surface.

12 The analytical model proposed in this paper can be applied to study the wave attenuation by the
13 floating breakwaters consisting of a float and an OWC. The wave power absorption obtained by
14 using the potential flow theory in this paper may be overestimated without consideration of water
15 viscous effect. Such viscous effect on the hybrid WEC device might be investigated by using
16 physical experiments in the future. The present work concentrates on analysis of the performance
17 of a two-dimensional hybrid WEC. Analytical study on the power extraction of a three-
18 dimensional hybrid WEC will be reported elsewhere.

19 **Acknowledgements**

20 The research was supported by the National Natural Science Foundation of China (51679124,
21 51479092), China Postdoctoral Science Foundation (Grant No. 2016M601041, 2017T100085)
22 and Tsinghua National Laboratory for Information Science and Technology.

23 **Appendix A. Expression of the generalized excitation forces in** 24 **terms of the radiated wave's far-field coefficients**

25 Since $\Phi_R^{(L)}$ ($L=1, 2, 3$) is the spatial velocity potential due to unit amplitude velocity oscillation of
26 the float in mode L , the component in mode L of the generalized normal vector n_L can be written
27 as

$$28 \quad n_L = \frac{\partial \Phi_R^{(L)}}{\partial n}, \quad (\text{A1})$$

29 therefore, Eq. (20) can be rewritten as

$$30 \quad F_e^{(L)} = -i\omega\rho \int_{S_1} (\Phi_1 + \Phi_D) \frac{\partial \Phi_R^{(L)}}{\partial n} ds = -i\omega\rho \int_{S_1} \left(\Phi_1 \frac{\partial \Phi_R^{(L)}}{\partial n} + \Phi_D \frac{\partial \Phi_R^{(L)}}{\partial n} \right) ds. \quad (\text{A2})$$

31 According to Green's theorem (Falnes, 2002), we have

$$1 \quad \int_{S_1} \left(\Phi_D \frac{\partial \Phi_R^{(L)}}{\partial n} - \Phi_R^{(L)} \frac{\partial \Phi_D}{\partial n} \right) ds = - \int_{S_{\pm\infty}} \left(\Phi_D \frac{\partial \Phi_R^{(L)}}{\partial n} - \Phi_R^{(L)} \frac{\partial \Phi_D}{\partial n} \right) ds = 0, \quad (\text{A3})$$

2 where $S_{\pm\infty}$ represents the boundaries at infinite, i.e., $x = \pm \infty$.

3 Hence, together with employment of the boundary condition of wave diffraction at wetted
4 surface, i.e., $\partial \Phi_D / \partial n = -\partial \Phi_1 / \partial n$, we have

$$5 \quad F_e^{(L)} = -i\omega\rho \int_{S_1} \left(\Phi_1 \frac{\partial \Phi_R^{(L)}}{\partial n} + \Phi_R^{(L)} \frac{\partial \Phi_D}{\partial n} \right) ds = -i\omega\rho \int_{S_1} \left(\Phi_1 \frac{\partial \Phi_R^{(L)}}{\partial n} - \Phi_R^{(L)} \frac{\partial \Phi_1}{\partial n} \right) ds, \quad (\text{A4})$$

6 which is one way of formulating the so-called Haskind relation.

7 If we reuse Green's theorem, wave excitation forces can be written as

$$8 \quad F_e^{(L)} = i\omega\rho \int_{S_{\pm\infty}} \left(\Phi_1 \frac{\partial \Phi_R^{(L)}}{\partial n} - \Phi_R^{(L)} \frac{\partial \Phi_1}{\partial n} \right) ds. \quad (\text{A5})$$

9 The incident wave potential is generally given as:

$$10 \quad \Phi_1 = -\frac{igAe^{ikx} \cosh[k(z+h)]}{\omega \cosh(kh)} = -\frac{igAe^{ikx} Z_1(z)}{\omega Z_1(0)}. \quad (\text{A6})$$

11 After inserting Eqs. (11), (14) and (A6) into Eq.(A5),

$$12 \quad \begin{aligned} F_e^{(L)} &= i\omega\rho \left[\int_{S_{+\infty}} \left(\Phi_1 \frac{\partial \Phi_R^{(L)}}{\partial n} - \Phi_R^{(L)} \frac{\partial \Phi_1}{\partial n} \right) ds + \int_{S_{-\infty}} \left(\Phi_1 \frac{\partial \Phi_R^{(L)}}{\partial n} - \Phi_R^{(L)} \frac{\partial \Phi_1}{\partial n} \right) ds \right] \\ &= i\omega\rho \left[\int_{S_{+\infty}} \left(ik\Phi_1\Phi_R^{(L)} - ik\Phi_R^{(L)}\Phi_1 \right) ds + \int_{S_{-\infty}} \left(-ik\Phi_1\Phi_R^{(L)} - ik\Phi_R^{(L)}\Phi_1 \right) ds \right] \\ &= i\omega\rho(-2ik) \int_{-h}^0 \left[\left(-\frac{igAe^{ikx} Z_1(z)}{\omega Z_1(0)} \right) \left(A_{1,l}^{(L)} e^{-ikx} Z_1(z) \right) \right]_{x=-\infty} dz \\ &= \frac{-2i\rho g A k h A_{1,l}^{(L)}}{Z_1(0)} \end{aligned} \quad (\text{A7})$$

13 For the excitation volume flux $F_e^{(4)}$, using the free surface boundary conditions of incident and
14 diffracted potentials, its expression as given in Eq. (21) can be written as:

$$15 \quad F_e^{(4)} = \int_{x_{R,2}}^{x_{L,3}} \frac{\partial(\Phi_1 + \Phi_D)}{\partial z} \Big|_{z=0} dx = -i\omega\rho \int_{x_{R,2}}^{x_{L,3}} (\Phi_1 + \Phi_D) \frac{i\omega}{\rho g} \Big|_{z=0} dx. \quad (\text{A8})$$

1 With the employment of the free surface boundary condition of $\Phi_R^{(4)}$ inside the OWC chamber,
 2 i.e., Eq. (2), and Green's theorem to Φ_D and $\Phi_R^{(4)}$ in a similar way as given in Eq. (A3), we have

$$\begin{aligned}
 F_e^{(4)} &= -i\omega\rho \int_{x_{R,2}}^{x_{L,3}} (\Phi_I + \Phi_D) \left(\frac{\partial \Phi_R^{(4)}}{\partial z} - \frac{\omega^2}{g} \Phi_R^{(4)} \right) \Big|_{z=0} dx \\
 &= -i\omega\rho \int_{x_{R,2}}^{x_{L,3}} \left(\Phi_I \frac{\partial \Phi_R^{(4)}}{\partial z} - \Phi_R^{(4)} \frac{\partial \Phi_I}{\partial z} \right) \Big|_{z=0} dx
 \end{aligned} \tag{A9}$$

4 For the unit normal at either water surface or wetted surface of structures in this paper is defined
 5 pointing into the fluid region, thus for the mean water level inside the chamber, $\partial/\partial z = -\partial/\partial n$.
 6 Using $\partial/\partial z = -\partial/\partial n$ at the mean water level and applying Green's theorem to Φ_I and $\Phi_R^{(4)}$, we
 7 have

$$\begin{aligned}
 F_e^{(4)} &= i\omega\rho \int_{x_{R,2}}^{x_{L,3}} \left(\Phi_I \frac{\partial \Phi_R^{(4)}}{\partial n} - \Phi_R^{(4)} \frac{\partial \Phi_I}{\partial n} \right) \Big|_{z=0} dx = -i\omega\rho \int_{S_{\pm\infty}} \left(\Phi_I \frac{\partial \Phi_R^{(4)}}{\partial n} - \Phi_R^{(4)} \frac{\partial \Phi_I}{\partial n} \right) ds \\
 &= -i\omega\rho (-2ik) \int_{-h}^0 \left[\left(-\frac{igAe^{ikx}}{\omega} \frac{Z_1(z)}{Z_1(0)} \right) \left(A_{1,1}^{(4)} e^{-ikx} Z_1(z) \right) \right] \Big|_{x=-\infty} dz \\
 &= \frac{2i\rho g A k h A_{1,1}^{(4)}}{Z_1(0)}
 \end{aligned} \tag{A10}$$

9 References

- 10 Boccotti, P., 2007. Caisson breakwaters embodying and OWC with a small opening- Part I:
 11 Theory. *Ocean Engineering*. 34, 806-819.
- 12 Chen, T., Wu, B., Li, M., 2017. Flume experiment study on capture width ratio of a new
 13 backward bent duct buoy with a pentagon buoyancy cabin. *Ocean Engineering*. 141, 12-17.
- 14 Deng, Z.Z., Huang, Z.H., Law, A.W.K., 2014. Wave power extraction from a bottom-mounted
 15 oscillating water column converter with a V-shaped channel. *Proceedings of the Royal
 16 Society A*. 470: 20140074.
- 17 Elhanafi, A., Fleming, A., Macfarlane, G., et al., 2016. Numerical energy balance analysis for an
 18 onshore oscillating water column-wave energy converter. *Energy*. 116 (Part 1), 539-557.
- 19 Elhanafi, A., Fleming, A., Macfarlane, G., et al., 2017. Underwater geometrical impact on the
 20 hydrodynamic performance of an offshore oscillating water column-wave energy converter.
 21 *Renewable Energy*. 105, 209-231.
- 22 Evans, D.V., 1982. Wave-power absorption by systems of oscillating surface pressure
 23 distributions. *Journal of Fluid Mechanics*. 114, 481-499.
- 24 Evans, D.V., Porter, R., 1995. Hydrodynamic characteristics of an oscillating water column
 25 device. *Applied Ocean Research*. 17, 155-164.

1 Falnes, J., 2002. Ocean waves and oscillating systems- linear interactions including wave-energy
2 extraction. Cambridge: Cambridge University Press.

3 Falnes, J., McIver, P., 1985. Surface wave interactions with system of oscillating bodies and
4 pressure distributions. *Applied Ocean Research*. 7(4), 225-234.

5 He, F., Huang, Z., 2017. Characteristics of orifices for modelling nonlinear power take-off in
6 wave-flume tests of oscillating water column devices. *Journal of Zhejiang University-
7 Science A*. 18(5), 329-345.

8 He, F., Huang, Z., Law, A.W.K., 2013. An experimental study of a floating breakwater with
9 asymmetric pneumatic chambers for wave energy extraction. *Applied Energy*. 106, 222-231.

10 He, F., Leng, J., Zhao, X., 2017. An experimental investigation into the wave power extractions
11 of a floating box-type breakwater with dual pneumatic chambers. *Applied Ocean Research*.
12 67, 21-30.

13 Heath, T.V., 2012. A review of oscillating water columns. *Philosophical Transactions of the
14 Royal Society A*. 370, 235-245.

15 Iturrioz, A., Guanache, R., Lara, J.L., et al., 2015. Validation of OpenFOAM for oscillating water
16 column three-dimensional modeling. *Ocean Engineering*. 107, 222-236.

17 López, I., Pereiras, B., Castro, F., et al., 2014. Optimisation of turbine-induced damping for an
18 OWC wave energy converter using a RANS-VOF numerical model. *Applied Energy*. 127,
19 105-114.

20 López, I., Pereiras, B., Castro, F., et al., 2016. Holistic performance analysis and turbine-induced
21 damping for an OWC wave energy converter. *Renewable Energy*. 85, 1155-1163.

22 Malara, G., Arena, G., 2013. Analytical modelling of an U-Oscillating Water Column and
23 performance in random waves. *Renewable Energy*. 60, 116-126.

24 Morris-Thomas, M. T., Irvin, R.J., Thiagarajan, K. P., 2007. An investigation into the
25 hydrodynamic efficiency of an oscillating water column. *Journal of Offshore Mechanics and
26 Arctic Engineering*. 129(4), 273-278.

27 Ning, D., Wang, R., Zhang, C., 2017. Numerical simulation of a dual-chamber oscillating water
28 column wave energy converter. *Sustainability*. 9, 1599. doi:10.3390/su9091599

29 Ning, D.Z., Shi, J., Zou, Q.P., et al., 2015. Investigation of hydrodynamic performance of an
30 OWC (oscillating water column) wave energy device using a fully nonlinear HOBEM
31 (higher-order boundary element method). *Energy*. 83, 177-188.

32 Noad, I., Porter, R., 2017. Wave energy absorption by a shallow-draughted rectangular barge of
33 oscillating water columns. *Proceedings of the 12th European Wave and Tidal Energy
34 Conference*. 27th Aug-1st Sept, 2017, Cork, Ireland. 651, pp. 1-9.

35 Rezanejad, K., Bhattacharjee, J., Guedes Soares, C., 2013, Analytical and numerical study of
36 nearshore multiple oscillating water columns. *Proceedings of the ASME 2013 32ND
37 International Conference on Ocean, Offshore and Arctic Engineering*. June 9-14, 2013,
38 Nantes, France. pp. 1-8.

39 Rezanejad, K., Bhattacharjee, J., Guedes Soares, C., 2015, Analytical and numerical study of
40 dual-chamber oscillating water columns on stepped bottom. *Renewable Energy*. 75, 272-
41 282.

42 Sarmiento, A.J.N.A., 1992. Wave flume experiments on two-dimensional oscillating water
43 column wave energy devices. *Experiments in Fluids*. 12, 286-292. Sheng, W, Alcorn, R.,
44 Lewis, A., 2014. Assessment of primary energy conversions of oscillating water columns. I.

1 Hydrodynamic analysis. *Journal of Renewable and Sustainable Energy*. 6,053113(2014);
2 DOI: 10.1063/1.4896850.

3 Sarmiento, A.J.N.A., Falcão, A.F.O., 1985. Wave generation by an oscillating surface-pressure
4 and its application in wave-energy extraction. *Journal of Fluid Mechanics*. 150, 467-485.

5 Zhang, Y., Zou, Q.P., Greaves, D., 2012. Air-water two-phase flow modelling of hydrodynamic
6 performance of an oscillating water column device. *Renewable Energy*. 41, 159-170.

7 Zheng, S., and Zhang, Y., 2016. Wave diffraction and radiation by multiple rectangular floaters.
8 *Journal of Hydraulic Research*. 54:1, 102-115.

9 Zheng, Y.H., You, Y.G., Shen, Y.M., 2004. On the radiation and diffraction of water waves by a
10 rectangular buoy. *Ocean Engineering*. 31, 1063-1082.

11